WITHDRAWN: Molecular Identification of Plant Growth-Promoting Rhizobacteria and Their Antiphytopathogenic Compounds by LC MS TOF Analysis

SMITHA Thomas

zmita80@gmail.com

St.Teresa's College https://orcid.org/0000-0003-2172-3251

Lizzy Mathew

St.Teresa's College

Article

Keywords: PGPR, LC-MS-TOF, Anti-phytopathogenic, IAA production, Sustainable agriculture

Posted Date: March 26th, 2025

DOI: https://doi.org/10.21203/rs.3.rs-6083519/v1

Additional Declarations: There is **NO** Competing Interest.

EDITORIAL NOTE:

The full text of this preprint has been withdrawn by the authors due to author disagreement with the posting of the preprint. Therefore, the authors do not wish this work to be cited as a reference. Questions should be directed to the corresponding author.

Molecular Identification of Plant Growth-Promoting Rhizobacteria and Their Antiphytopathogenic Compounds by LC MS TOF Analysis

[1*]Smitha Thomas and [2] Lizzy Mathew

[1*,2]Department of Botany, St.Teresa's College (Autonomous), Ernakulam, affiliated to M.G.University, Kottayam, Kerala, India.682 011.

*email: zmita80@gmail.com

Abstract

Beneficial Plant Growth-Promoting Rhizobacteria (PGPR) colonize plant roots and enhance plant growth through various mechanisms. This study assessed the role of PGPR in sustainable agriculture. Bacterial isolates were collected from various districts of Kerala, followed by isolation and screening. Ten of 90 strains were selected for comprehensive *in vitro* characterization, including morphological, biochemical and molecular identification. LC-MS-TOF analysis identified 37 anti-phytopathogenic compounds in positive and 11 in negative modes, confirming their strong biocontrol potential. These findings highlight their potential to enhance plant growth and disease resistance, supporting eco-friendly agricultural practices.

Key words: PGPR; LC-MS-TOF; Anti-phytopathogenic; IAA production; Sustainable agriculture

1. Introduction

A diverse yet substantial population of microorganisms thrives in the rhizosphere, the surrounding plant roots influenced by root exudates[6]. Rhizosphere-colonising bacteria, known as plant growth-promoting rhizobacteria (PGPR), stimulate plant growth through direct and indirect mechanisms[31]. The root microbiome, consisting of beneficial bacterial communities in the rhizoplane and root endosphere, plays a crucial role in plant growth facilitation[54]. Plants release carbon molecules into the soil, making microbial populations in the rhizosphere 100-1000 times higher than in bulk soil[28,29]. The root system provides structural stability, absorbs water and nutrients, stores essential compounds, supports vegetative growth and interacts with diverse microbial populations[34]. Microbial communities metabolise plant-secreted compounds, including organic acids, phyto-siderophores, sugars, vitamins, amino acids, nucleosides and mucilage[10,16]. Root exudates serve as the primary carbon source in soil, supporting up to 10^{10} bacteria per gram[32]. The rhizome-microbiome refers to microbial communities residing in plant roots[24,40]. PGPR enhance plant performance through direct mechanisms such as phytohormone production, biological nitrogen fixation and solubilisation of essential nutrients (P, K, Zn), along with siderophore-mediated iron chelation[39,65]. Indirect mechanisms include resistance to abiotic stress and suppression of plant pathogens[30]. Several bacterial genera, including *Acinetobacter, Agrobacterium, Arthrobacter, Azotobacter, Azospirillum, Burkholderia, Bradyrhizobium, Rhizobium, Frankia, Serratia, Thiobacillus, Pseudomonas* and *Bacillus* are recognised as PGPR[20]. Beneficial plant-microbe interactions occur as symbiotic alliances, where both partners share benefits and costs[3,4], or associative symbioses, which involve close cooperation[58]. Mutualistic interactions result in specialised structures such as nodules in Fabaceae-rhizobia symbiosis or arbuscules in mycorrhizal relationships[9]. Rhizobacteria colonise plant root surfaces and sometimes internal root tissues, enhancing plant health and growth[60,67]. While PGPR research has traditionally focused on aerial plant parts due to their economic importance, recent studies highlight the significance of root traits in ecosystem functioning[69]. Understanding PGPR-mediated root trait modifications could improve agroecosystem efficiency and contribute to sustainable agriculture[46].

A comprehensive understanding of root system growth and function is critical for achieving a second Green Revolution, essential for global food security[42]. PGPR optimise root traits that enhance soil resource utilisation, increasing crop productivity in sustainable agricultural systems[5,44]. Various *Bacillus* species enhance plant growth, yield and biomass by improving nutrient availability, solubilising essential nutrients for better uptake and synthesizing key compounds such as indole-3-acetic acid (IAA), which facilitates nutrient absorption. Additionally, these bacteria contribute to nitrogen fixation, phosphorus solubilisation and phytohormone production, further stimulating plant growth. PGPR enhance crop quality by increasing the synthesis of IAA, gibberellins, siderophores and various cell surface components, ultimately promoting plant health and productivity[63]. Today's farming methods depend heavily on helpful microorganisms in agriculture, underscoring the necessity of moral standards and optimal microbial utilisation techniques. Standardized procedures throughout the

microbiological supply chain guarantee constant efficacy and quality, improving agricultural output and environmental health. By adopting this strategy, we can address current challenges while fostering a microbiome revolution that strengthens food system resilience and supports sustainable agriculture for present and future generations[59].

2. Materials and Method

2.1 Rhizosphere Soil Sampling

Rhizosphere soil samples were collected from healthy vegetable plants across several locations in Kerala, India. Sampling was conducted in September 2021 from different districts. Plants were uprooted and the bulk of the soil was removed by gentle shaking. Soil samples were then collected in sterile containers and transported to the laboratory for further analysis. Microbial isolation was carried out using the standard serial dilution technique. After thorough cleaning, 1 g of soil and root sections were mixed with 9 mL of sterile physiological saline (pH 7.2). The rhizosphere soil suspensions were vortexed gently for 10 minutes and allowed to rest for 20 minutes. A 100 µL aliquot of each progressively diluted suspension was spread on nutrient agar plates, incubating at 30 ± 2°C for 2–3 days. Morphologically distinct colonies were selected, subcultured on nutrient agar plates and preserved in 20% glycerol at -20°C. For further research, 90 rhizobacterial isolates with distinctive colony characteristics were chosen for detailed evaluation.

2.2 Plant Growth-Promoting Properties

Indole Acetic Acid (IAA) Screening

After inoculating 10 millilitres of nutritional broth with 0.3% (w/v) L-tryptophan, PGPR isolates were cultured for 48 hours at 28°C. After centrifuging the cultures for 15 minutes at 12,000 rpm, the supernatant was examined for IAA. Initially, 1 mL of the culture supernatant was mixed with 2 mL of Salkowski reagent (35% $HClO_4$, 0.5 M $FeCl_3$) and incubated in the d k for 30 minutes. The development of a red colour indicated a positive result, while an uninoculated growth medium served as a negative control.

Phosphate Solubilization

Phosphate solubilization ability was assessed using Pikovskaya medium supplemented with 2.4 mg/mL romophenol Blue. The medium was inoculated with bacterial isolates and incubated for 48 hours. The colony's use of the medium's tricalcium phosphate was demonstrated by the development of a yellow zone surrounding it.

ACC Deaminase Production

Isolates were inoculated into D salt's minimal medium containing 0.2% (w/v) ammonium sulfate $(NH_4)_2SO_4(NH_4)_2$ $O_4(NH_4)_2SO_4$. After 4 days of incubation, bacterial growth in the medium indicated a positive result for ACC deaminase production.

Nitrogen Fixation

Bacterial isolates were inoculated into Jensen's medium and incubated for 4 days. The appearance of a blue colour around colony growth confirmed nitrogen fixation.

Ammonia Production

Isolates were inoculated into peptone water and incubated at room temperature for two days. Subsequently, 2-3 drops of Nessler's reagent were a added to the culture. The formation of a brown colouration indicated a positive result, while an uninoculated growth medium served as a negative control.

Siderophore Production

As indicators, siderophore production was assessed using Blue Agar CAS medium, which contains Chrome Azurol S CAS) and Hexa Decyl Tri Methyl Ammonium Bromide (HDTMA). To prepare the medium, 100 mL of MM9 salt solution was mixed with 750 mL of distilled water. 32.24 g of Piperazine-N, N-bis (2-ethanesulfonic acid) (PIPES) was dissolved, adjusting the pH to below 5. After adding 15 g of agar, the solution was cooled to 50°C and autoclaved. A sterile 20% glucose solution

(10 mL) and a sterile Casamino acid solution (30 mL) were added to the MM9/PIPES combination. Then, 100 mL of Blue Dye solution was mixed against the glass wall. Bacterial isolates were inoculated o to CAS medium and incubated at 28°C for one day. The presence of a yellowish-orange halo around the colonies indicated siderophore production.

HCN Production

HCN production was evaluated using nutrient agar plates supplemented with 4.4 g/L glycine. A filter paper strip was soaked in 0.5% picric acid and 2% sodium carbonate (Na_2CO_3) inside the Petri dish lid. After being sealed, the plates were incubated for four days at 30°C. An uninoculated growth media was used as a control and a yellow-to-red colour shift on the filter paper signified a successful outcome.

Potassium Solubilization

Potassium solubilization was tested using an Aleksandrow agar medium. Bacterial isolates were inoculated and incubated for seven days. The formation of a clear zone around the colonies indicated successful potassium solubilization.

Morphological Characterization of PGPR Isolates

Ten P PR isolates P5-KRS-II, P35-NLIII, P45-C2I, P55-NLII, P65-Ja, P67-Ma, P70-Ac, P73-Ia, P75-Ca and P80-Fa, were selected for identification. Phenotypic characterization was performed following *Bergey's Manual of Determinative Bacteriology*.

Gram's Staining

A bacterial inoculum was smeared onto a sterilized glass slide using an inoculating, air-dried and heat-fixed loop. After 30 seconds of crystal violet treatment, the slide was cleaned with distilled water and air-dried. After adding Gram's iodine for 60 seconds, the mixture was washed with 95% ethyl alcohol to remove any remaining colour. Safranin was applied for 30 seconds before a final rinse with distilled water. The slide was air-dried and observed under a microscope to determine the Gram reaction.

Motility Test

The motility of bacterial isolates was assessed using the hanging drop technique. A small amount of vaseline was applied to the four corners of a cover slip. A loopful of the bacterial culture from the nutrient broth was placed in the centre of the cover-slip. A deep session slide was pressed against it and then inverted, allowing the drop to hang freely. The slide was examined using a compound microscope to evaluate motility, which is defined as active movement in a specific direction.

2.3 Biochemical Tests

Kovac's (Indole) Test

To perform the Kovac's (Indole) test, bacterial isolates were inoculated into 5 mL of MRVP broth and incubated at 37°C for 24 hours. After incubation, 2-3 drops of Ehrlich Kovács reagent were added to the culture tubes. The tubes were gently shaken for 30-60 seconds and left to stand at room temperature for at least 30 minutes. The development of a red color indicated a positive result, while a pale color signified a negative reaction.

Methyl Red Test

To prepare the Methyl Red reagent, 0.1 g of Methyl Red was dissolved in 300 mL of ethanol (95%) and mixed with 200 mL of deionized water to obtain a 0.05% (wt/vol) solution in 60% ethanol (vol/vol). The solution was stored at 4°C for further use. A loopful of bacterial culture was inoculated into 5 mL of MRVP broth and incubated for 24 hours. After incubation, 2.5 mL of the culture was transferred to a fresh test tube and a few drops of Methyl Red reagent were added. The development of a red color indicated a positive result, whereas a yellow color indicated a negative result.

Voges-Proskauer Test

For the Voges-Proskauer test, bacterial isolates were inoculated into 5 mL of MRVP broth and incubated at 37°C for 24 hours. After incubation, 0.2 mL of Barritt's reagent B and 0.6 mL of Barritt's reagent A were added to the culture. The tubes were then gently shaken for 30-60 seconds and left at

room temperature for 30 minutes. The appearance of a red color indicated a positive result, whereas the presence of a yellow color indicated a negative result.

Citrate Test

For the citrate test, the PGPR isolates were streaked onto Simmon's citrate agar slants and incubated at room temperature for 24-48 hours. A positive result was indicated by a color change of the agar slant from green to blue.

Oxidase Test

In the oxidase test, a strip of Whatman No. 1 filter paper was soaked in 1% Tetramethyl-p-phenylenediamine dihydrochloride and freeze-dried. The strip was then moistened with distilled water and a bacterial colony was applied to the moist area using a platinum loop. The appearance of a deep purple color within 5-10 seconds indicated a positive result. A delayed positive reaction was noted if the color change occurred between 10-60 seconds, whereas no color change within 60 seconds indicated a negative result.

Catalase Test

To perform the catalase test, a drop of 3% hydrogen peroxide was added to a 5 µL bacterial culture streaked onto a sterilized glass slide. The formation of oxygen bubbles indicated a positive result, suggesting the presence of the catalase enzyme.

Urease Test

For the urease test, all the ingredients, except for urea, were dissolved in 100 mL of distilled water and sterilized by autoclaving at 121°C and 15 psi for 15 minutes. After cooling, 100 mL of filter-sterilized urea base was added to the solution aseptically and mixed thoroughly. Approximately 4-5 mL of the prepared medium was dispensed into test tubes and a loopful of bacterial culture was inoculated into each tube. The tubes were then incubated at 35-37°C for 4-7 days to observe urease activity.

Nitrate Reduction Test

For the nitrate reduction test, nitrate broth was prepared and inoculated with actively growing bacterial cultures. The tubes were incubated at 28°C for 2-3 days. Before adding reagents, the broth was examined for N_2 gas production. Following this, 6-8 drops of Nitrite reagent A (Sulfanilic acid) and 6-8 drops of Nitrite reagent B (α-naphthylamine) were added. The appearance of a red color indicated nitrate reduction activity.

Gelatin Liquefaction Test

To perform the gelatin liquefaction test, gelatin deep tubes were inoculated with 4-5 drops of a 24-hour broth culture or by stabbing the medium 4-5 times (0.5 inches deep) with a 24-hour-old bacterial colony. The tubes were incubated at 35-37°C in ambient air for up to 14 days. Liquefaction was checked daily by removing the tube from the incubator and placing it at 4°C. An uninoculated control tube was refrigerated alongside the test tube. If the control tube remained solid while the test tube showed liquefaction, the result was considered positive.

2.4 Molecular Identification of Selected PGPR

Genomic DNA was isolated from selected bacterial strains using the methods described below to facilitate molecular identification.

Isolation of Genomic DNA

Genomic DNA was extracted using the conventional Chloroform: Isoamyl alcohol method. A few distinct bacterial colonies were maintained separately and nutrient broth was inoculated with the cultures and incubated for 12 to 16 hours. After incubation, 1 mL of the overnight culture was transferred to a sterile micro-centrifuge tube and centrifuged at 12,000 rpm for 10 minutes to collect the cells. The resulting pellet was re-suspended in 1 mL of 0.85% (w/v) NaCl solution and the supernatant was discarded after centrifugation. Following this, 600 µL of lysis buffer was added to the pellet along with 7 µL of Proteinase K. The mixture was vortexed and incubated at 65°C for one hour. An equal volume of Chloroform: Isoamyl alcohol (24:1) was added to the solution and the tubes were gently inverted and stirred for five minutes. The samples were then centrifuged at 12,000 rpm for 15 minutes. The aqueous phase was carefully collected into a fresh microcentrifuge tube without disturbing the lower phase or the interface. The Chloroform: Isoamyl alcohol extraction was repeated and the aqueous phase was collected once again. To facilitate DNA precipitation, an equal volume of ice-cold isopropanol and 1/10th volume of 3M sodium acetate (pH 5.2) were added to the aqueous phase. The tubes were gently inverted three to five times and centrifuged at room temperature for five minutes. The supernatant was removed and the DNA pellet was washed twice with 70% isopropanol. The tubes were then placed in a vacuum desiccator or a dry area for one hour to ensure complete drying of the DNA pellet.

Preparation of 0.8% Agarose Gel and Electrophoresis

To prepare a 1X TBE electrophoresis buffer (Tris-Borate-EDTA), 4 mL of 50X TBE was diluted in 200 mL of distilled water. To prepare the agarose gel, 0.4 g of agarose was dissolved in 50 mL of 1X TBE buffer by boiling until the agarose was completely dissolved. Once a clear solution was achieved, a 0.8% agarose gel was prepared. When the solution reached 50°C, it was mixed with 0.5 µg/mL of ethidium bromide as a staining dye. Meanwhile, a comb was placed in the electrophoresis gel mold, positioned 2 cm away from the cathode. The agarose solution, containing the staining dye, was poured into the center of the tank, ensuring no air bubbles were formed. The gel was allowed to cool and solidify at room temperature. Once the gel temperature reached 60°C, 1X TAE buffer was added to the gel tank until the buffer level reached approximately 0.5–0.8 cm above the gel surface. The comb was carefully removed to prevent damage to the wells. For loading, 2.5 µL of gel loading buffer was mixed with 25 µL of freshly extracted DNA samples. The samples were loaded into the wells of a 1% agarose gel along with 10 µL of control DNA. Electrophoresis was performed at 100 volts for 1–2 hours until the tracking dye (bromophenol blue) migrated to approximately three-fourths of the gel length. After electrophoresis, the DNA fragments were visualized using a gel documentation system.

16S rDNA Amplification by PCR

The extracted genomic DNA was used as a template for PCR amplification to determine the molecular identity of the bacterial isolates based on 16S rDNA sequences. The primers used for amplification were 16S-F (5'-AGAGTTTATCMTGG-3') and 16S-R (5'-ACCTTGTTACGACTT-3'), selected based on previous studies. PCR amplification was performed in a 25 µL reaction volume, containing 50 ng of template DNA, 10 pmol of each primer and 12 µL of Master Mix (TaKaRa). The amplification was conducted using a MyCycler thermal cycler (Bio-Rad, USA) with the following thermal cycling conditions:

Sequencing and Analysis of 16S rDNA

The amplified PCR product was purified and sequenced for further analysis. The obtained sequencing data were validated using BLAST (Zhang et al., 2000) to confirm the molecular identity of the isolates.

2.5 Characterization of the Antagonistic Compound

LC-MS -TOF analysis

The cyclohexane-ethyl acetate extract was dissolved in methanol and filtered through a 0.2 µm PTFE membrane before analysis. LC-MS analysis was performed using an ultra-high-performance liquid chromatography system (HR-LCMS-QTOF, Agilent Technologies, USA). Chromatographic separation was carried out using a ZORBAX Eclipse Plus C18 column (150 × 2.1 mm, 5 µm, Agilent). The

elution gradient was set using mobile phase A (0.1% formic acid in water) and mobile phase B (acetonitrile in 100% methanol). The gradient started with 5% B for the first minute, gradually increasing to 100% B over 25 minutes. This composition was maintained for five minutes before returning to 5% B within one minute, followed by re-equilibration for four minutes. The injection volume was 3 µLand the flow rate was maintained at 300 µL/min. For mass spectrometry, the MS1 acquisition method was used to capture both positive and negative ion Electrospray Ionization (ESI) mass spectra. The cone voltage was adjusted between 25 and 50 V to optimize ionization. The mass spectrometer parameters were set with a gas temperature of 250°C, a gas flow rate of 13 L/min. and a nebulizer pressure of 35 psi. Additionally, the sheath gas temperature was maintained at 300°C, with a sheath gas flow rate of 11 L/min. The MS1 data was processed using Agilent Mass Hunter Qualitative Analysis Software.

Description of components

The interpretation of the mass spectrum obtained from LC-MS-TOF and GC-MS analysis was conducted using the National Institute of Standards and Technology (NIST) database, which contains over 62,000 reference patterns. The mass spectrum of the unknown components was compared with the spectra of known compounds stored in the NIST library. Through this comparison, the name, molecular weight and chemical structure of the components present in the test materials were identified and confirmed.

3.Results

3.1 Plant growth promoting activities

PGPR enhance plant nutrition by improving nutrient uptake efficiency and accelerating development[26,35]. They expand root surface area, aiding absorption, while ion transporters regulate nutrient uptake[52,12]. Coordination between root growth regulators and ion transport maintains a steady nutrient supply[62]. PGPR improve nutrient availability through phosphate solubilization and nitrogen fixation[15]. Despite the abundance of soil phosphorus, much remains inaccessible due to fertilizer accumulation[47]. *Pseudomonas, Bacillus* and *Rhizobium* enhance phosphorus availability by releasing organic acids and enzymes[25,23]. While PGPR contribute to nitrogen fixation, its role in plant development remains debated[64,68]. Research on PGPR-mediated absorption is limited, but *Achromobacter* sp. has been shown to enhance nitrate and potassium uptake in canola[14,64]. In *Arabidopsis*, nitrate uptake varies over time, demonstrating the complexity of microbial influence[37,2]. Microbial-rich soils with high organic matter require less fertilizer due to enhanced nutrient cycling[11,21]. PGPR facilitate nutrient acquisition through root surface expansion, phosphate solubilization, siderophore production and HCN synthesis[41,66,27] **(Table 1-2).** Managing microbial activity is key to optimizing plant nutrition. This study identified ten isolates **(Table 3)** with *Pseudomonas fluorescens* (Fa) **(Fig.1)** and *Bacillus subtilis* (Ca) as PGPR **(Fig.2)** at the molecular level.

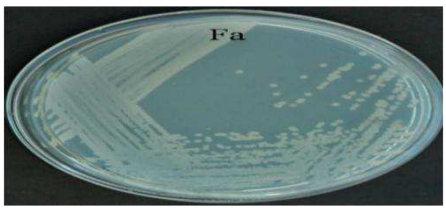

Fig.1. ***P. fluorescens*** **(P80)**

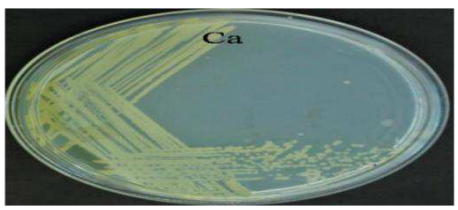

Fig.2. ***B.subtilis*** **(P75)**

Isolates	**PGP Features**							
	IAA	**P-Solublisati**	**Ammonia**	**N- Fixation**	**ACC Deamin**	**Siderophore**	**HCN**	**K-Solublisati**

		on			as			on
Fa	+	+	+	+	+	+	+	+
Ca	+	-	+	-	+	-	-	-

Table 1 Plant Growth Promoting Features

Tests	Catalase	Gram Staining	Motility	MR Test	VP TEST	Kovac's Indole	Citrate	Urease	Nitrate	Gelatin Liquefaction	Oxidase	Morphology of Isolates
Fa	+	-ve	-	-	-	-	+	+	-	+	+	**Rods**
Ca	+	+ve	-	+	-	-	+	-	+	+	-	**Rods**

Table 2 Biochemical characteristics of Isolates

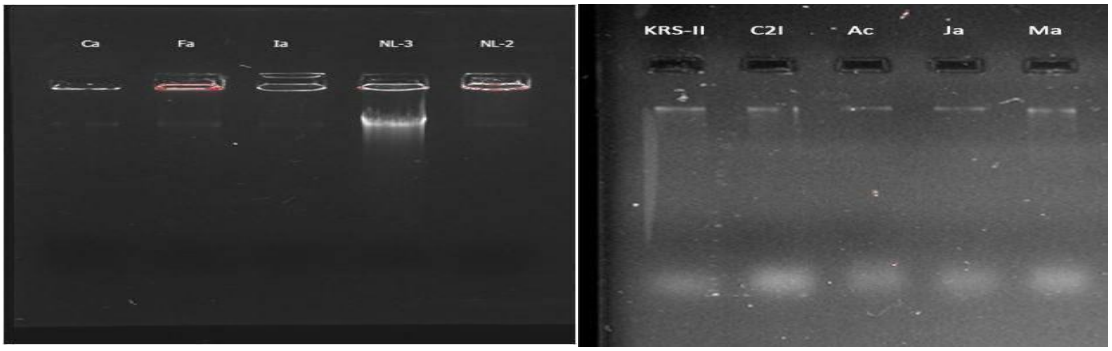

Fig. 3: Agarose Gel Electrophoresis image of IAA positive isolates: Lane 1: Ca; Lane 2: Fa; Lane 3: Ia; Lane4:NL-III; Lane 5: NL-II, Lane 6: KRS-II; Lane 7: C2I; Lane 8: Ac; Lane 9: Ja; Lane 10: Ma

Name of Samples	Host Plants	Places	No.of bps	% identity	Organisms
NLII	*Colocasia esculenta*	Kakkancheri, Kozhikode	610	99.02	*Burkholderia contaminan*
NLIII	*Vigna radiata*	Aluva, Ernakulam	529	99.43	*Pseudomonas viridiflava*
Ia	*Momordica charantia*	Peechadu, Idukki	1040	100	*Bacillus tequilensis*
Fa	*Amaranthus tricolor*	Rajakkadu, Idukki	807	100	*Pseudomonas fluorescens*
Ca	*Cucurbita moschata*	Murickassery, Idukki	871	100	*Bacillus subtilis*
KRSII	*Moringa oleifera*	Aluva, Kochi	863	100	*Enterobacter cloacae*
Ac	*Phaseolus vulgaris*	Rajakumari. Idukki	667	99.25	*Klebsiella quasipneumoniae*
Ja	*Solanum tuberosum*	Irumbupalam, Idukki	850	100	*Bacillus pumilus*
Ma	*Amorphophallus paeoniifolius*	Palarivattom, Kochi	902	100	*Pseudomonas fluorescens*
C21	*Benincasa hispida*	Kizhmadu, Aluva, Kochi	787	99.75	*Pseudomonas fluorescens*

Table 3: Identification of Rhizospheric bacteria

3.2 Identification of anti-phytopathogenic compounds by LC - QTOF MS

LC-MS QTOF (Liquid Chromatography-Mass Spectrometry Quadrupole Time-of-Flight) is a powerful analytical technique used to identify and characterize biomolecules, including metabolites, secondary metabolites and proteins in biological samples. This technique plays a crucial role in confirming the presence of key secondary metabolites involved in plant growth promotion and biocontrol. Additionally, it aids in the identification of anti-phytopathogenic compounds in *P.fluorescens*, supporting molecular findings from PCR analysis. Furthermore, LC-MS QTOF enables

the correlation of metabolite profiles with bioactivity data, providing valuable insights into the functional role of detected compounds. **(Fig. 4 to 5.11a; Table 4 and 5).**

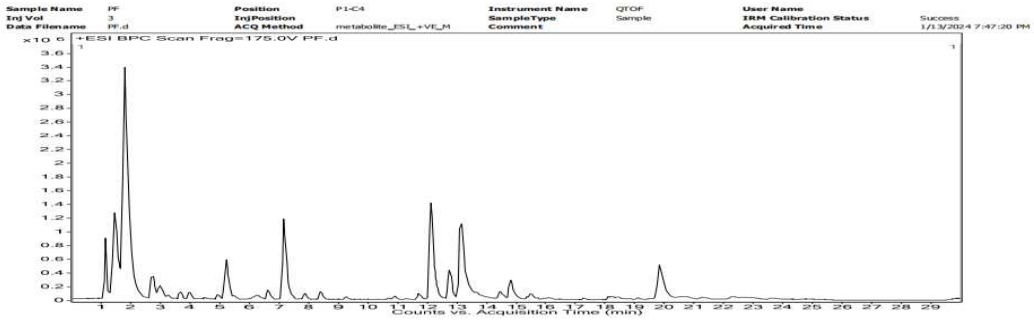

Fig. 4. LC - QTOF MS of Bioactive fractions in Positive mode

3.3.1. Anti-phytopathogenic compounds with Chemical Structure-Positive Mode

1. (2', 3'- Dihydroxyacetophenone)

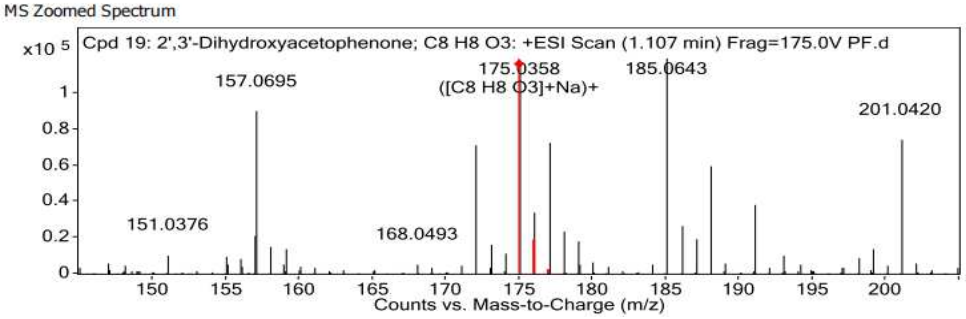

Fig. 4.1. LCMS-QTOF MS: 2', 3'-Dihydroxyacetophenone

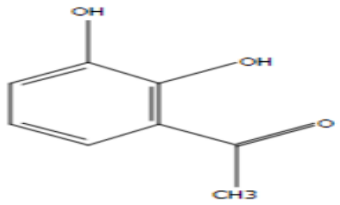

Fig. 4.1a: Structure of 2',3'-Dihydroxyacetophenone

2. Metsulfovax

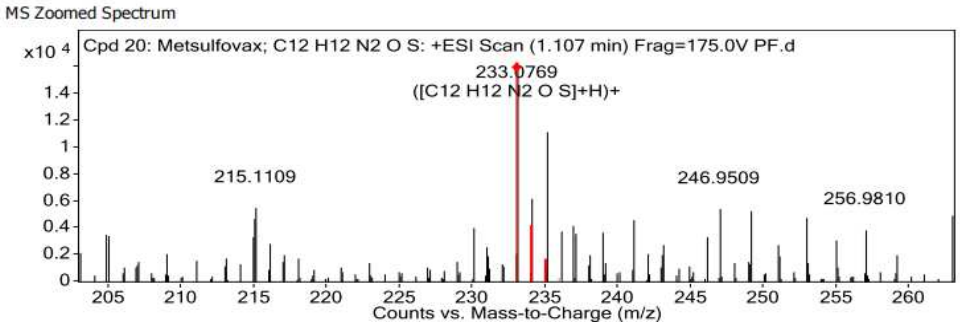

Fig. 4.2. Metsulfovax

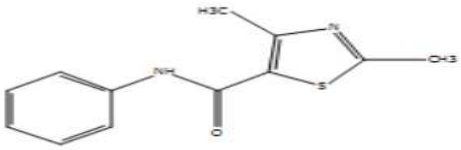

Fig. 4.2b. Structure of Metsulfovax

3. Hypoglycin

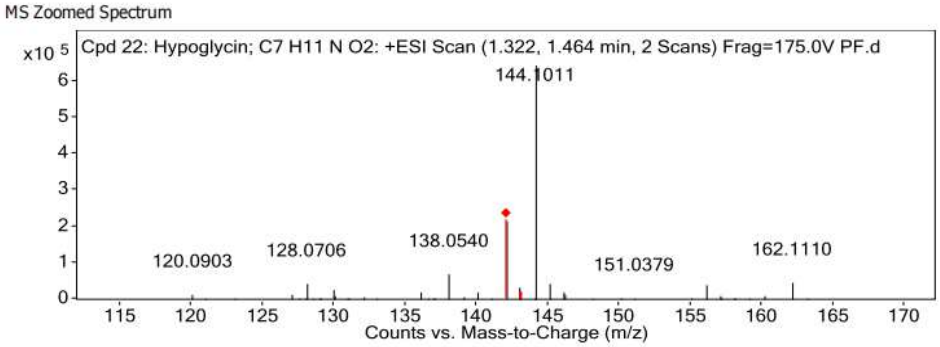

Fig. 4.3. Hypoglycin

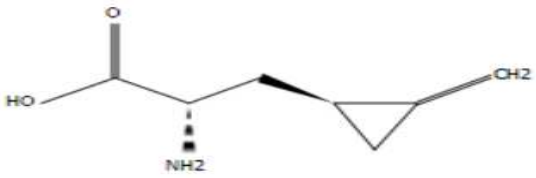

Fig. 4.3a. Structure of Hypoglycin

4. Carisoprodol

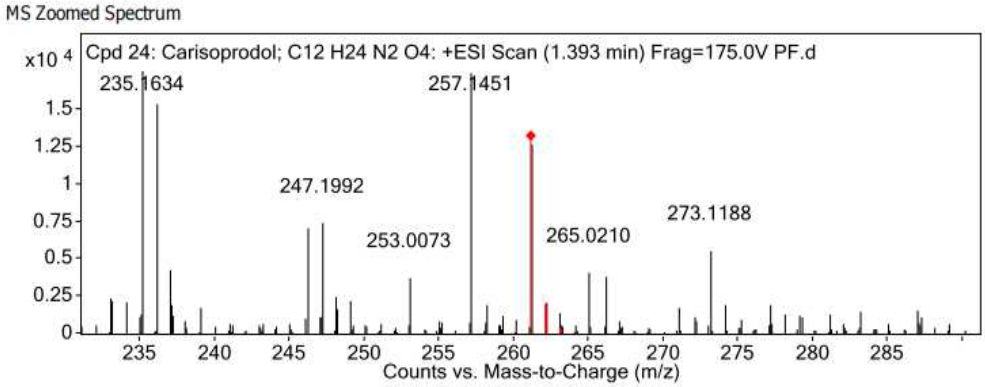

Fig. 4.4. Carisoprodol

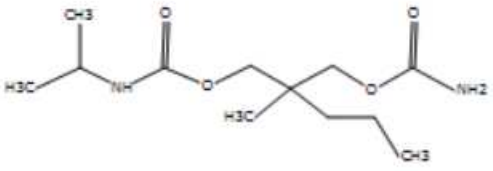

Fig. 4.4a. Structure of Carisoprodol

5.(3-beta,6-beta, Dihydroxynortropane)

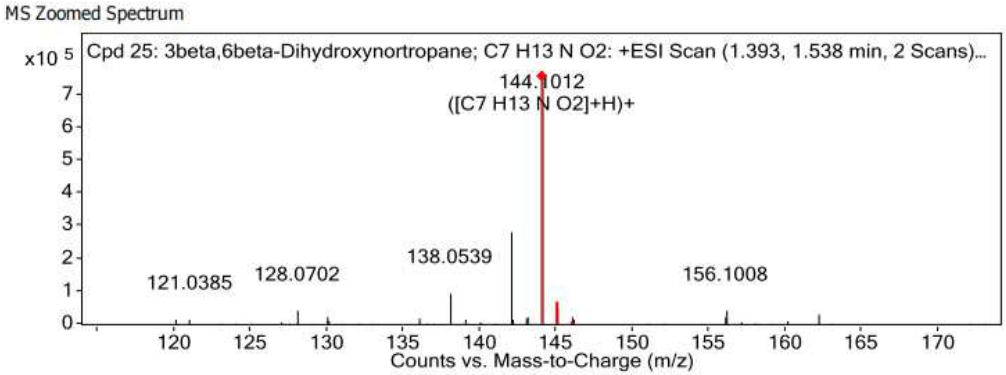

Fig. 4.5. (3-beta,6-beta, Dihydroxynortropane)

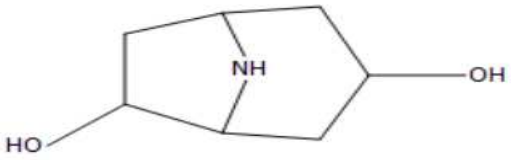

Fig. 4.5a. Structure of 3-beta,6-beta, Dihydroxynortropane

6. L-isoleucyl-L-proline

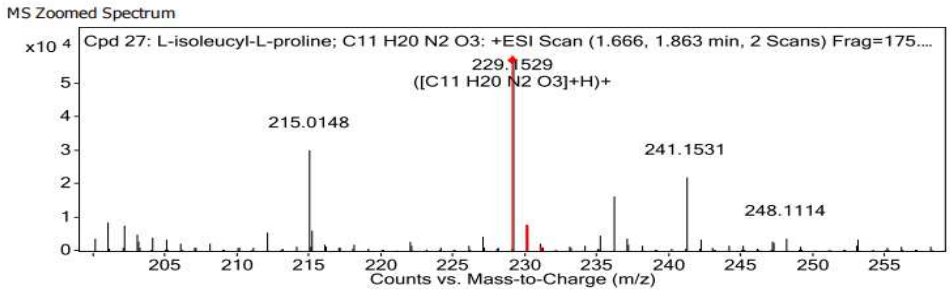

Fig. 4.6. L-isoleucyl-L-proline

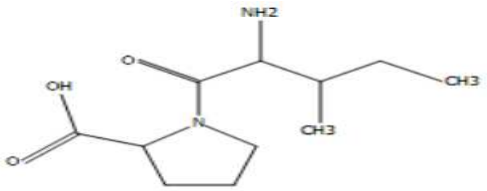

Fig. 4.6a Structure of L-isoleucyl-L-proline

7. Pirbuterol

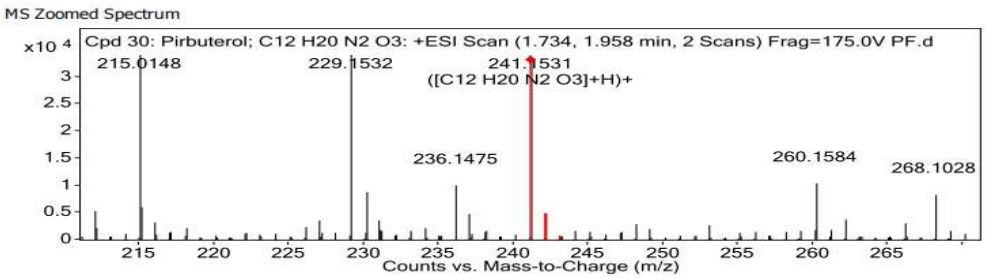

Fig. 4.7. Pirbuterol

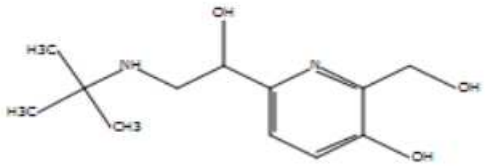

Fig. 4.7a. Structure of Pirbuterol

8. Procyanidin B7

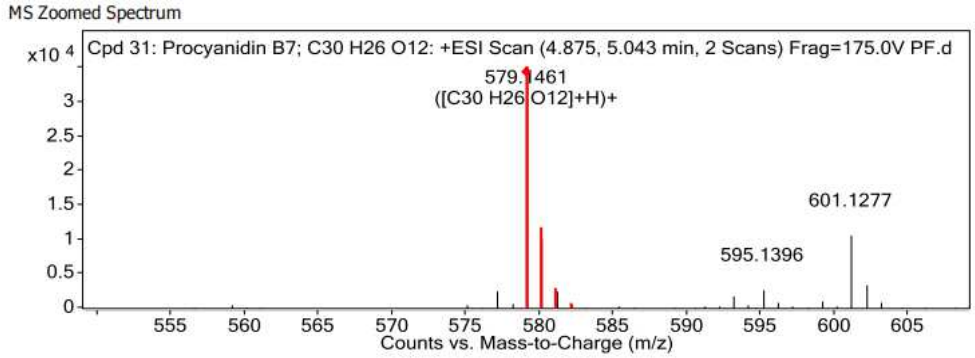

Fig. 4.8. Procyanidin B7

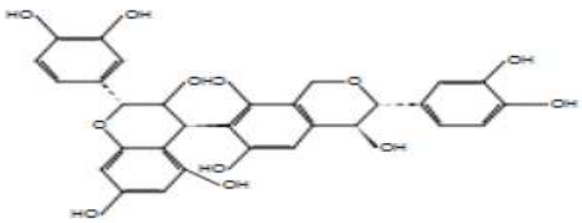

Fig. 4.8a. Structure of Procyanidin B7

9. Octylamine

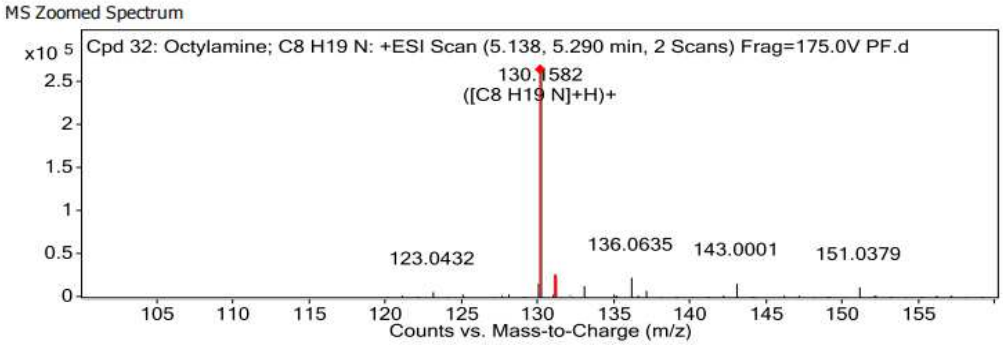

Fig. 4.9. Octylamine

Fig. 4.9a. Structure of Octylamine

10. Orotidine

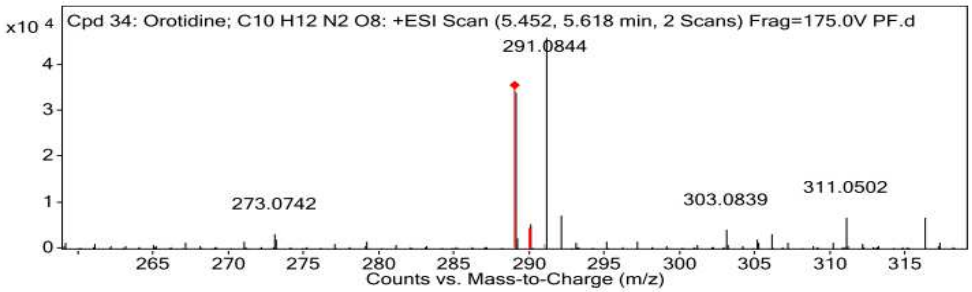

Fig. 4.10. Orotidine

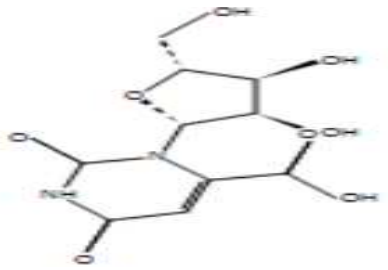

Fig: 4.10 a Structure of Orotidine

11. Minoxidil

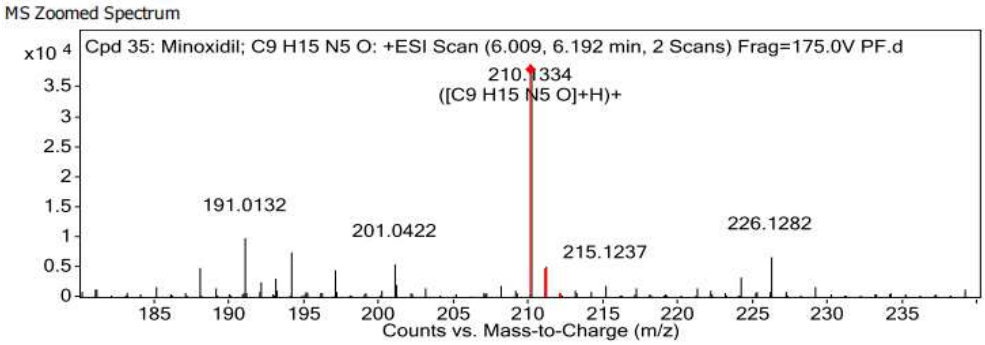

Fig. 4.11. Minoxidil

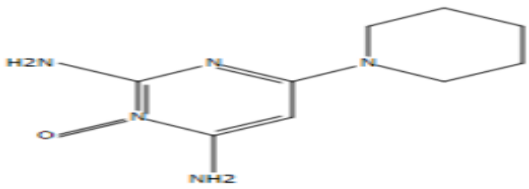

Fig. 4.11a. Structure of Minoxidil

12. Furanojaponin

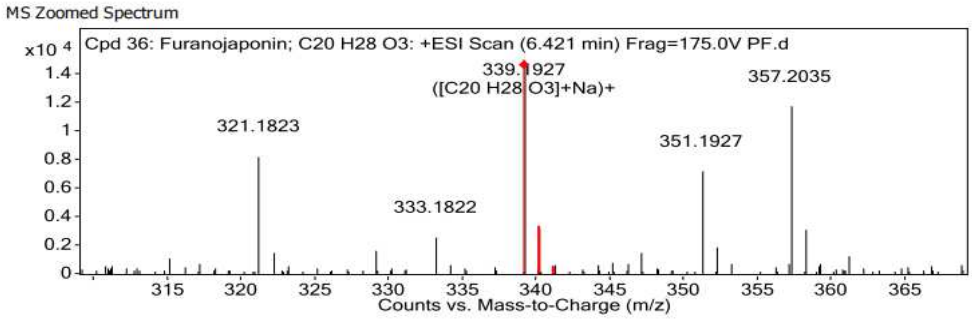

Fig. 4.12 Furanojaponin

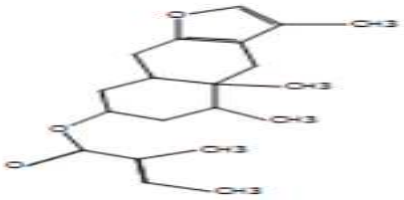

Fig. 4.12a. Structure of Furanojaponin

13. Erinapyrone C

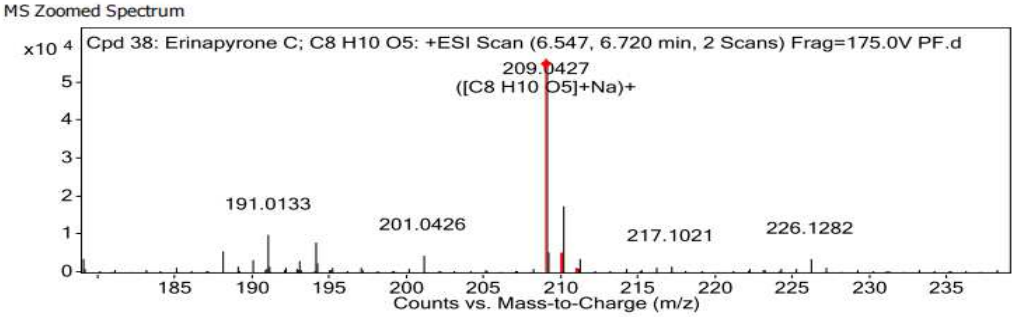

Fig.4.13. Erinapyrone C

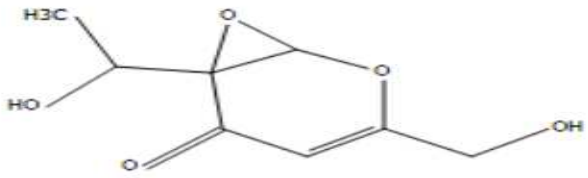

Fig. 4.13a. Structure of Erinapyrone C

14. (Z)-3-(1-Formyl-1-propenyl) pentanedioic acid

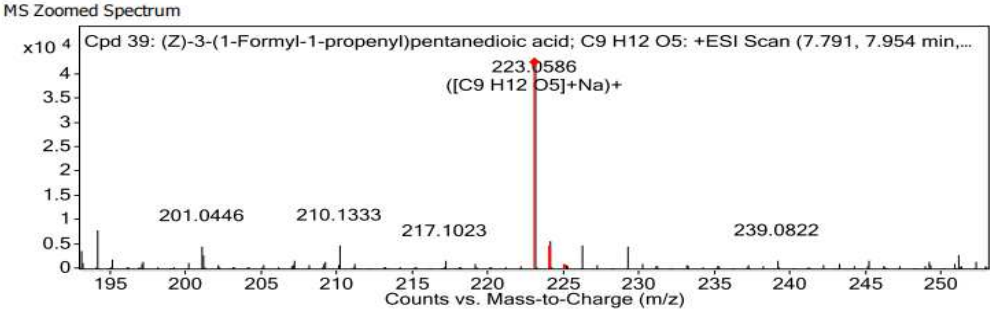

Fig. 4.14. (Z)-3-(1-Formyl- 1-propenyl) pentanedioic acid

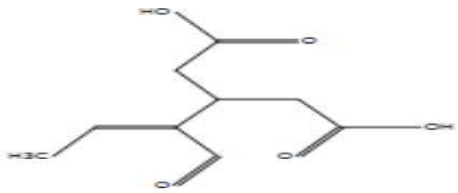

Fig. 4.14a. Structure of (Z)-3-(1-Formyl-1-propenyl) pentanedioic acid

15. 11beta,17beta-Dihydroxy-9alpha-fluoro-17alpha-methyl-5alpha-androstan-3-one

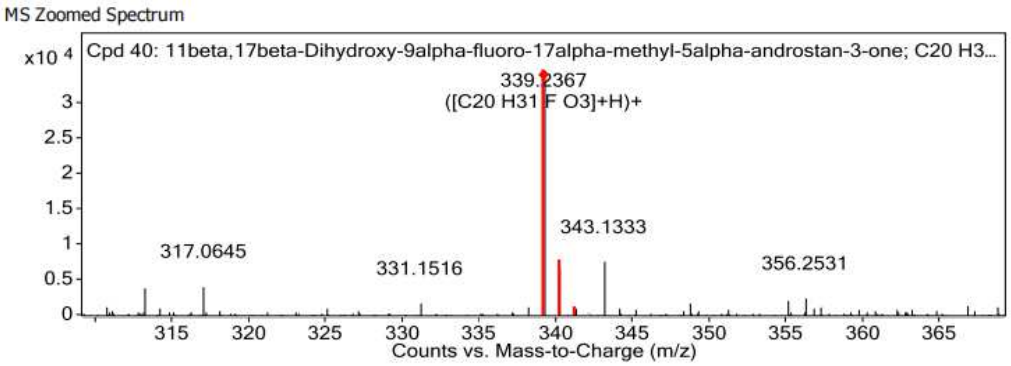

Fig. 4.15. (11beta,17beta-Dihydroxy- 9alpha-fluoro-17alpha-methyl-5alpha-androstan-3-one)

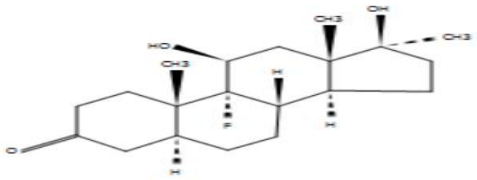

Fig. 4.15a. Structure of 11beta,17beta-Dihydroxy-9alpha-fluoro-17alpha-methyl-5alpha-androstan-3-one

16. Talampanel

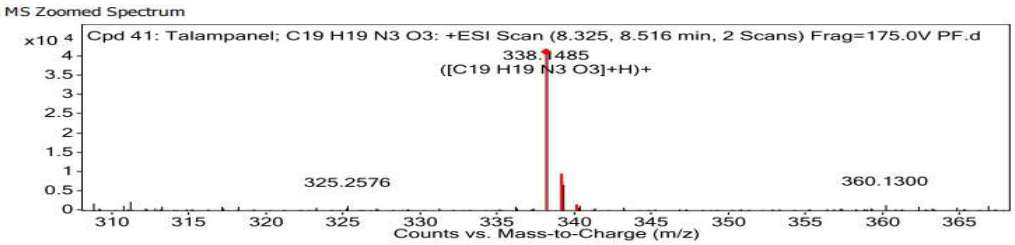

Fig. 4.16: Talampanel

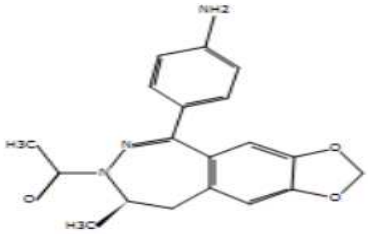

Fig. 4.16a: Structure of Talampanel

17. 6-sulfatoxymelatonin

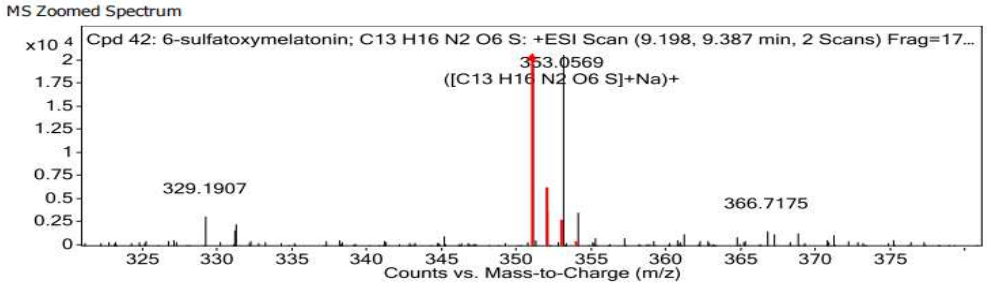

Fig. 4.17: 6-sulfatoxymelatonin

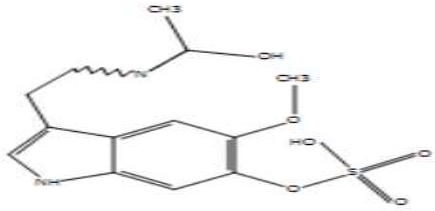

Fig. 4:17a: Structure of 6-sulfatoxymelatonin

18. Coriandrone E

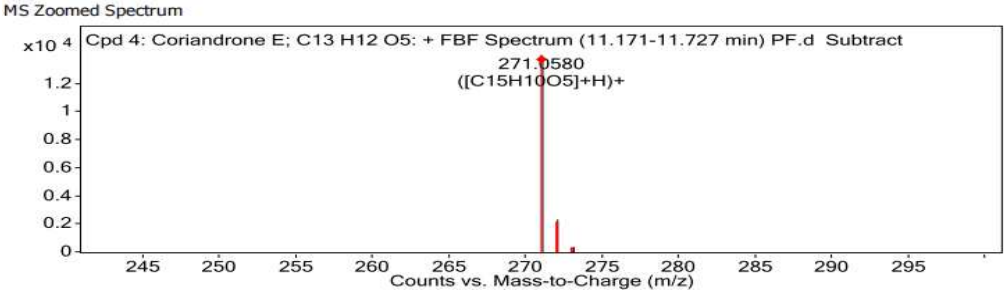

Fig. 4.18: Coriandrone E

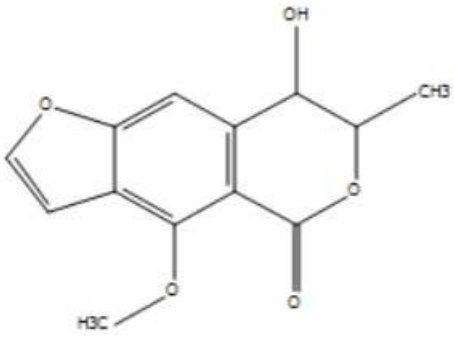

Fig. 4.18a: Structure of Coriandrone E

19. Sphinganine

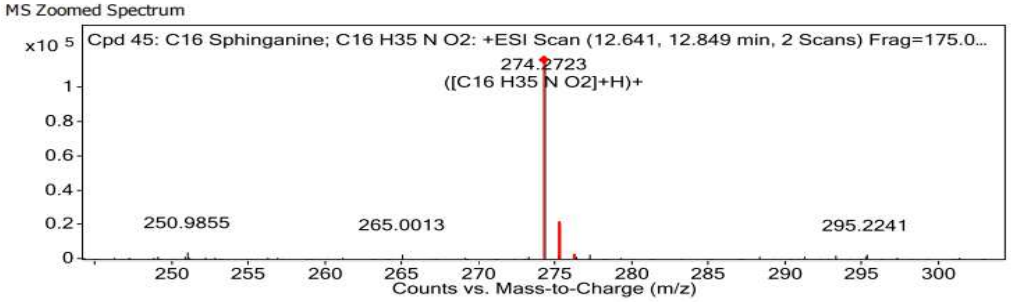

Fig. 4.19: Sphinganine

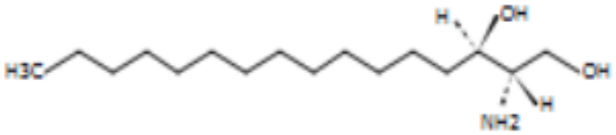

Fig. 4.19a: Structure of Sphinganine

20. Azafenidin

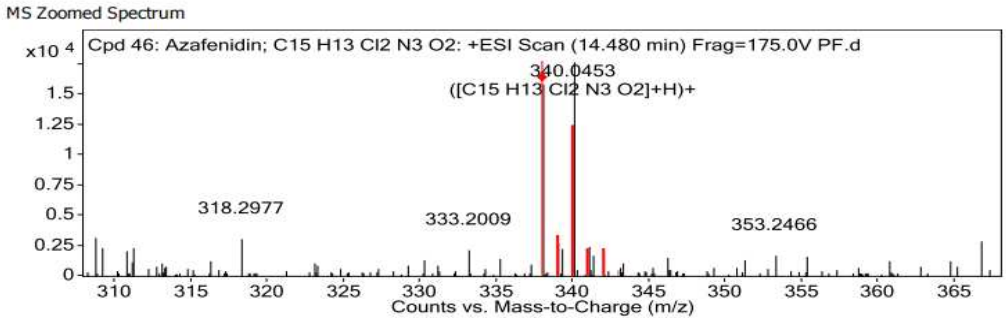

Fig. 4.20: LCMS-QTOF MS: Azafenidin

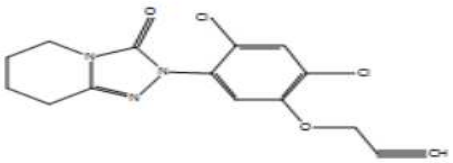

Fig. 4.20a: Structure of Azafenidin

21. 6-Hydroxypentadecanedioic acid

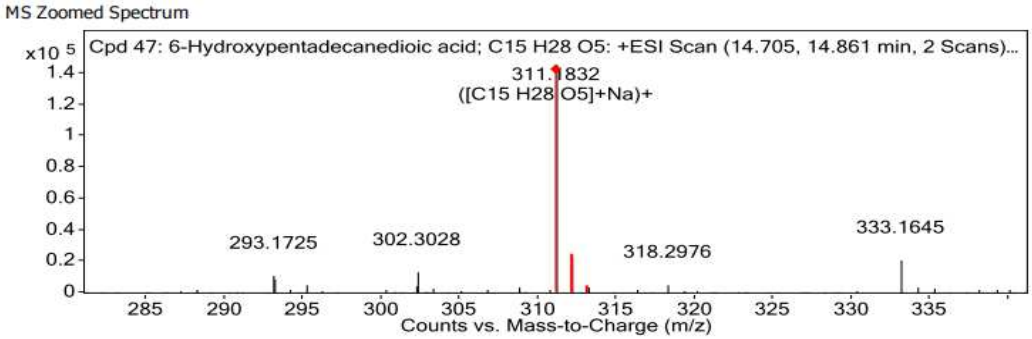

Fig. 4.21: 6-Hydroxypentadecanedioic acid

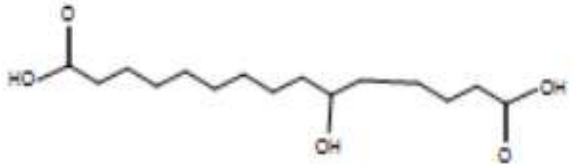

Fig. 4.21a: Structure of 6-Hydroxypentadecanedioic acid

22. Nigakilactone B

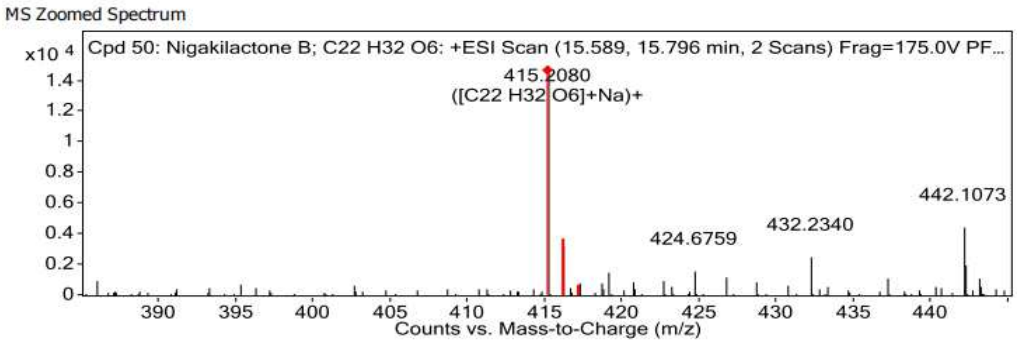

Fig. 4.22: Nigakilactone B

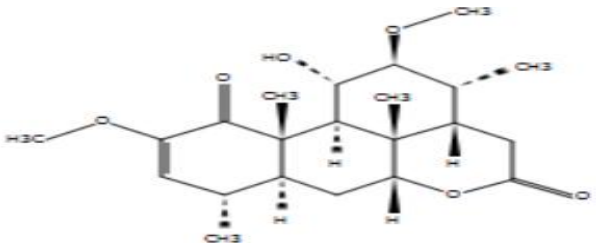

Fig. 4.22a: Structure of Nigakilactone B

23. Tropacocaine

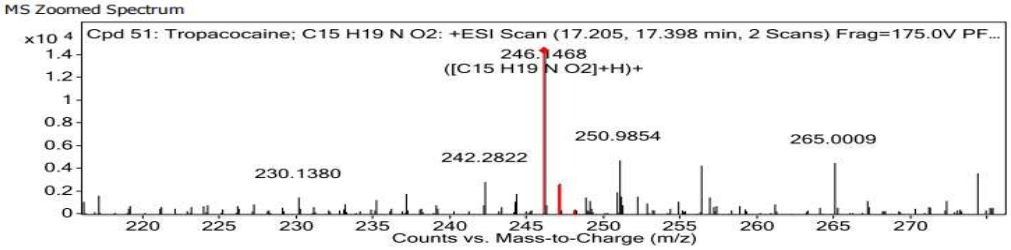

Fig: 4.23: Tropacocaine

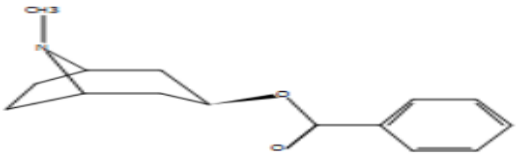

Fig: 4.23a: Structure of Tropacocaine

24. Brassicanal B

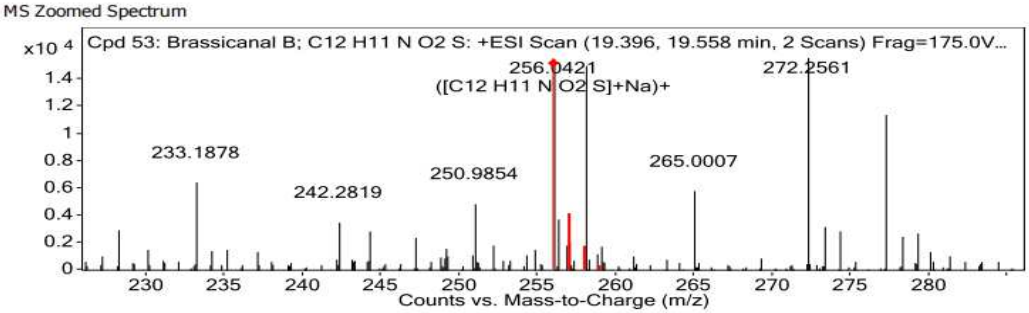

Fig. 4.24: Brassicanal B

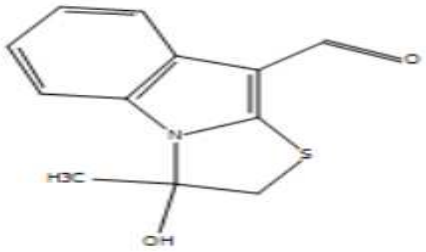

Fig. 4.24a: Structure of Brassicanal B

25. Carylophyllene oxide

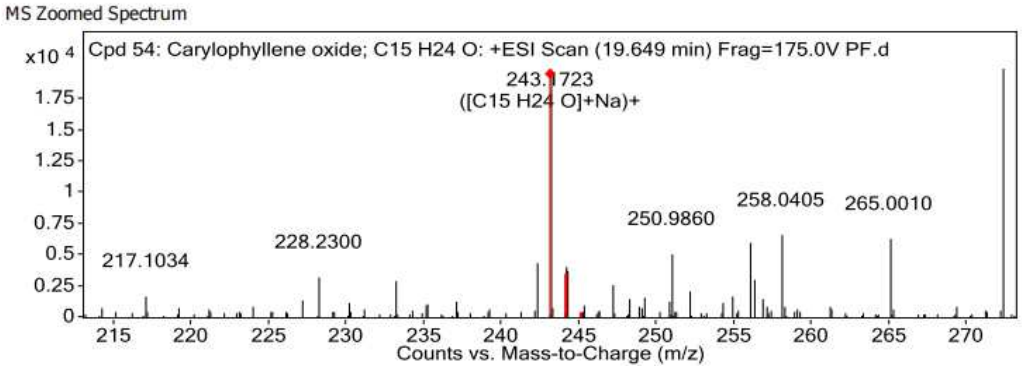

Fig. 4.25: Carylophyllene oxide

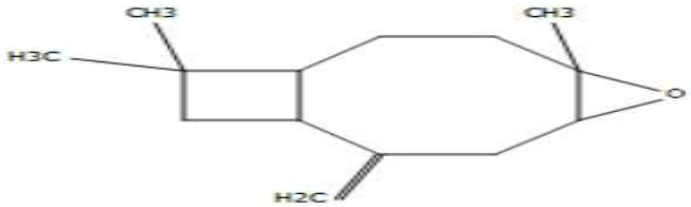

Fig. 4.25a: Structure of Carylophyllene oxide

26. Monomenthyl succinate

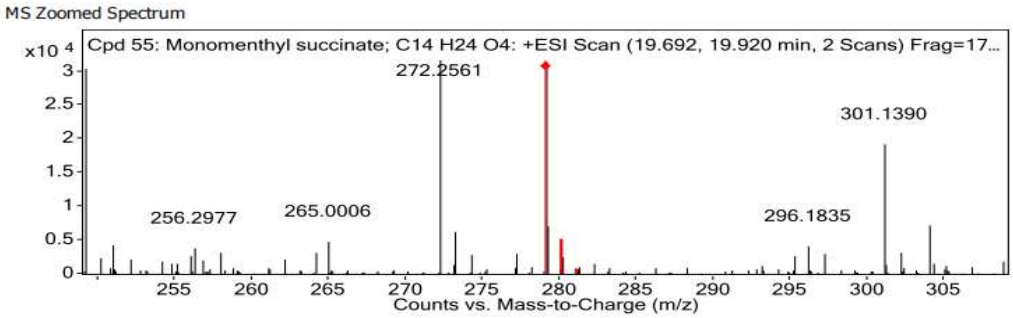

Fig. 4.26: Monomenthyl succinate

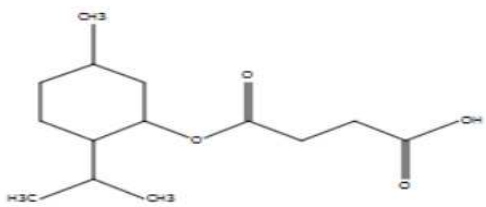

Fig. 4.26a: Structure of Monomenthyl succinate

27. 2-Methyl-1-phenyl-2-propanyl butyrate

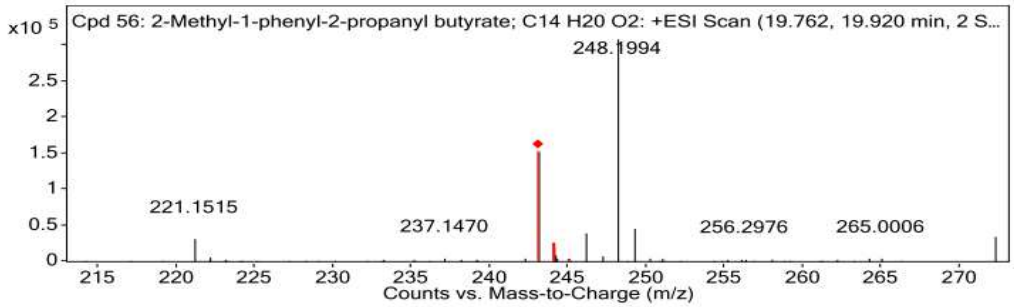

Fig. 4.27: 2-Methyl-1-phenyl-2-propanyl butyrate

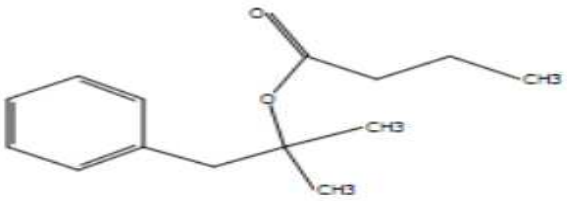

Fig. 4.27a: Structure of 2-Methyl-1-phenyl-2-propanyl butyrate

28. Eugenol

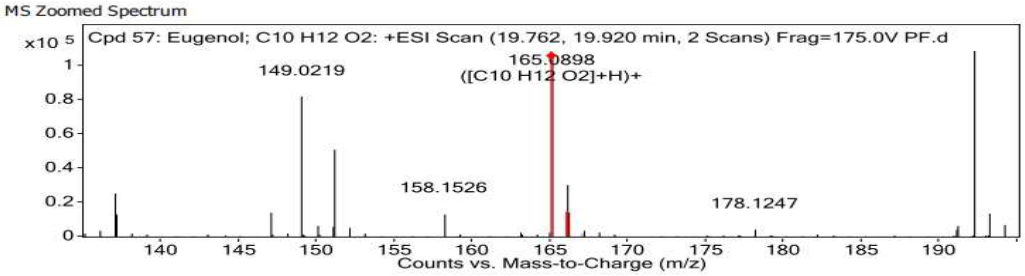

Fig. 4.28: Eugenol

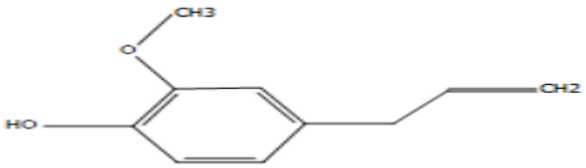

Fig. 4.28a: Structure of Eugenol

29. (E,E)-2,4-Decadienoic iso butylamide

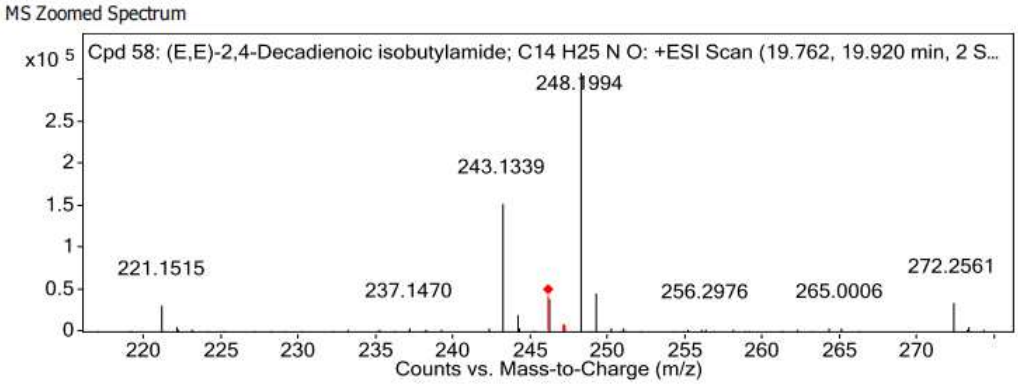

Fig. 4.29: (E,E)-2,4-Decadienoic iso butylamide

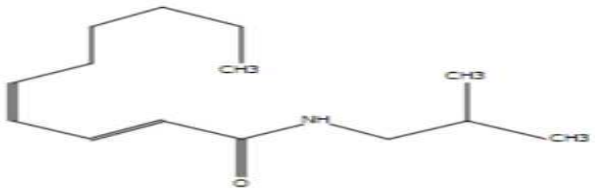

Fig. 4.29a: Structure of (E,E)-2,4-Decadienoic iso butylamide

30. 2-Amino-1,2-bis(p chlorophenyl) ethanol

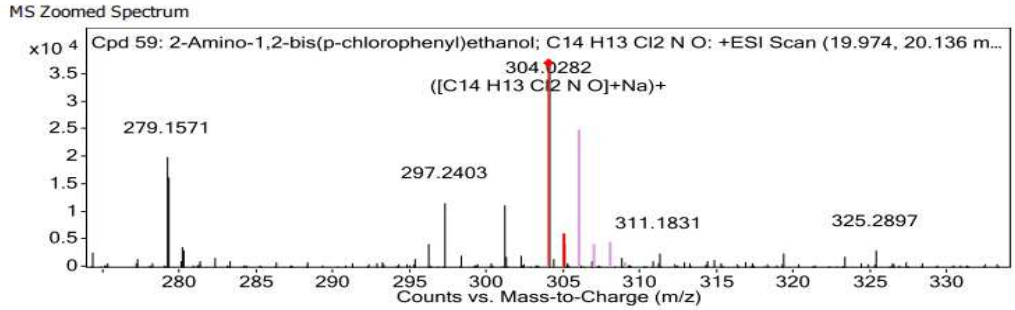

Fig. 4.30: 2-Amino-1,2-bis(p chlorophenyl) ethanol

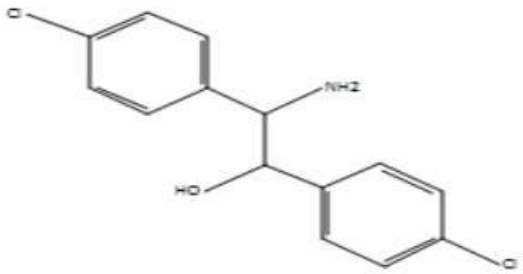

Fig.4.30a:Structure of 2-Amino-1,2-bis(p -chlorophenyl) ethanol

31. 2,6-Di-tert-butyl-4- ethyl phenol

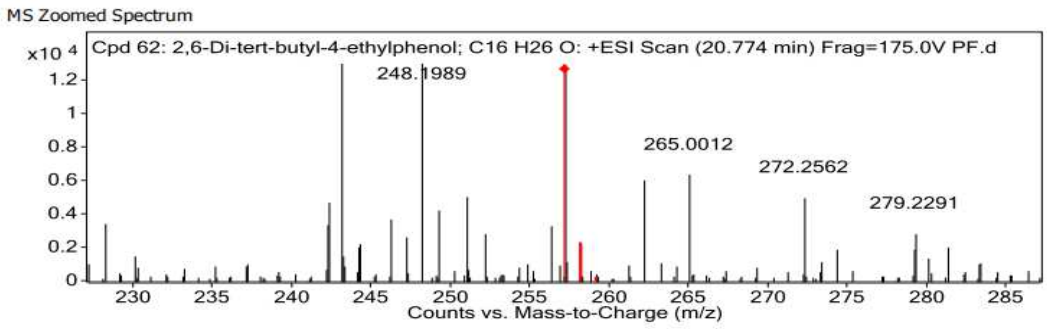

Fig. 4.31:2,6-Di-tert-butyl-4- ethyl phenol

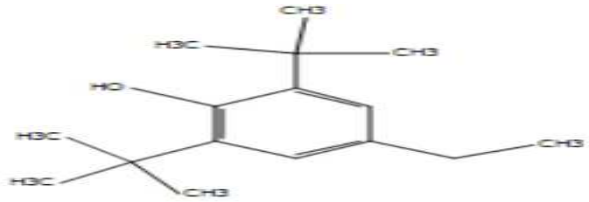

Fig. 4.31a Structure of 2,6-Di-tert-butyl-4- ethyl phenol

32. (2R)-3-(2Aminoethoxy)(hydroxy) phosphoryl-oxy)-2-(pentadecanoyloxy) propyl (13Z)-13-docosenoate

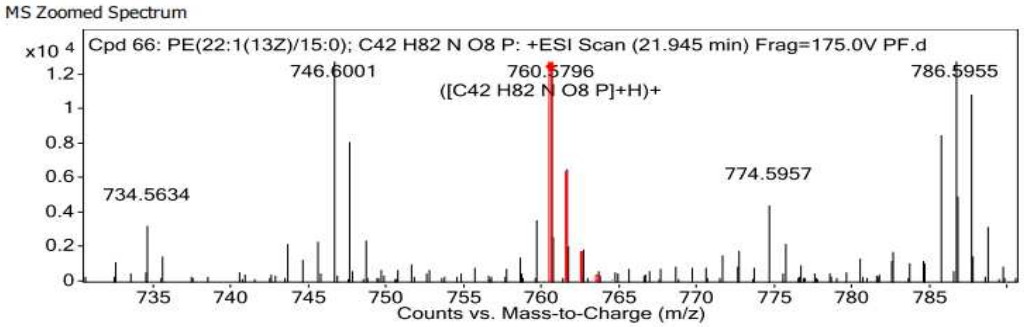

Fig. 4.32: (2R)-3 (2Aminoethoxy)-(hydroxy) -(phosphoryl-oxy)-2-(pentadecanoyloxy) propyl (13Z)-13-docosenoate

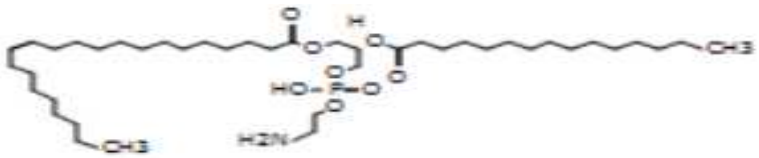

Fig. 4.32a: Structure of (2R)-3-(2Aminoethoxy)(hydroxy)- (phosphoryl-oxy}-2-(pentadecanoyloxy) propyl (13Z)-13-docosenoate

33. 9,10-Dihydroxy-12,13-epoxyoctadecanoate

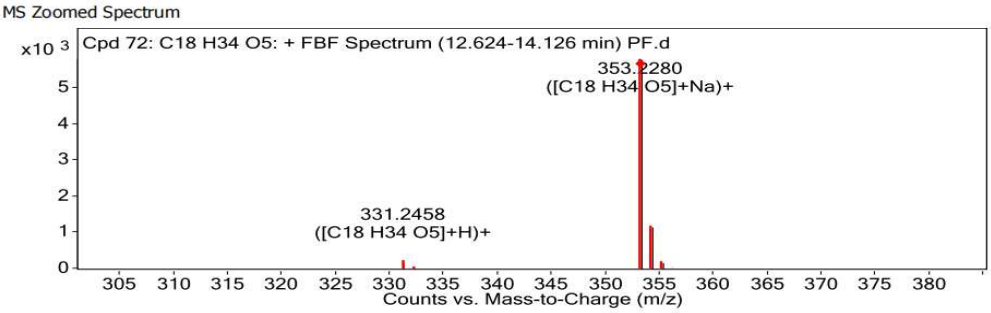

Fig. 4.33: 9,10-Dihydroxy-12,13-epoxyoctadecanoate

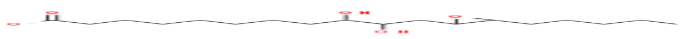

Fig. 4.33a: Structure of 9,10-Dihydroxy-12,13-epoxyoctadecanoate

34. Octadecanedioic acid

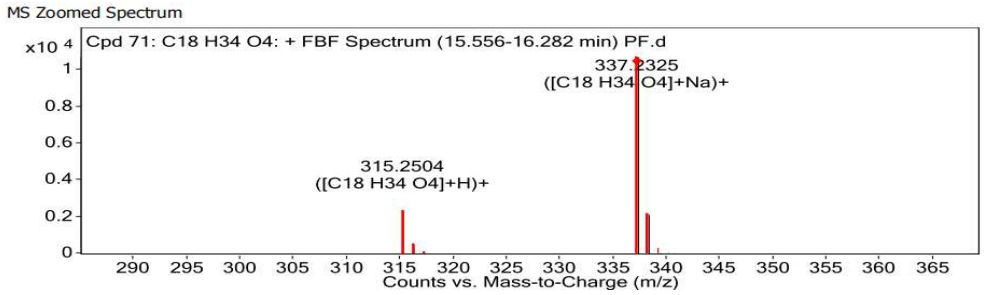

Fig. 4.34: Octadecanedioic acid

Fig. 4.34a Structure of Octadecanedioic acid

35. (Z)-13-Oxo-9-octadecenoic acid

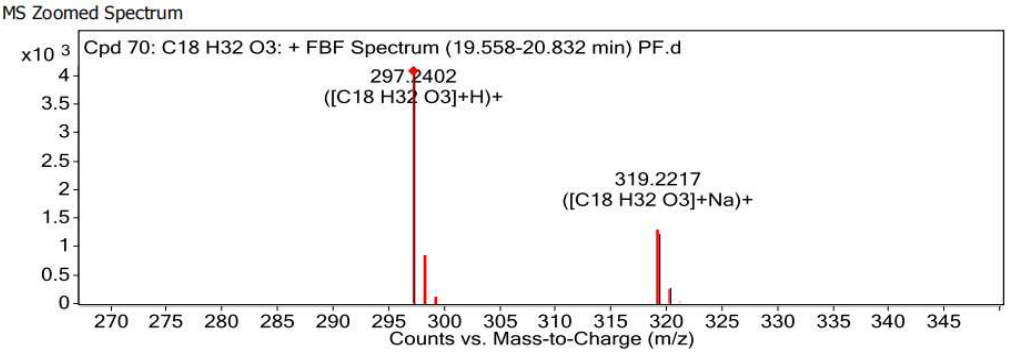

Fig. 4.35: (Z)-13-Oxo-9-octadecenoic acid

Fig. 4.35a: Structure of (Z)-13-Oxo-9-octadecenoic acid

36. Vanilpyruvic acid

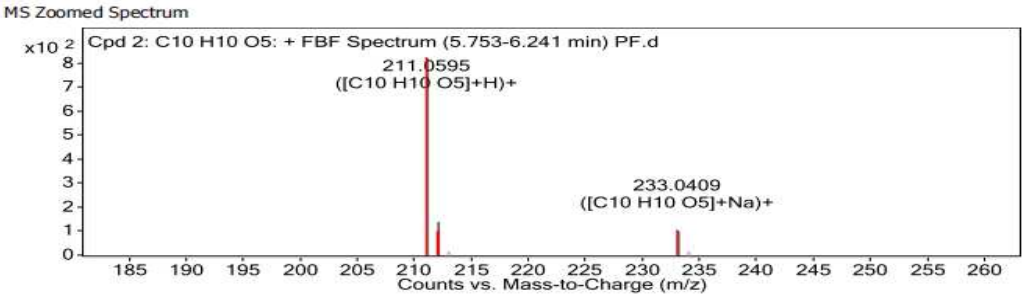

Fig. 4.36: Vanilpyruvic acid

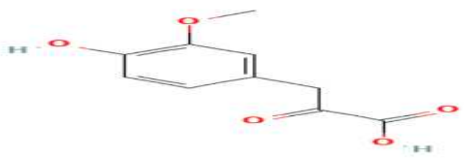

Fig. 4.36a: Structure of Vanilpyruvic acid

37. Palmitic acid

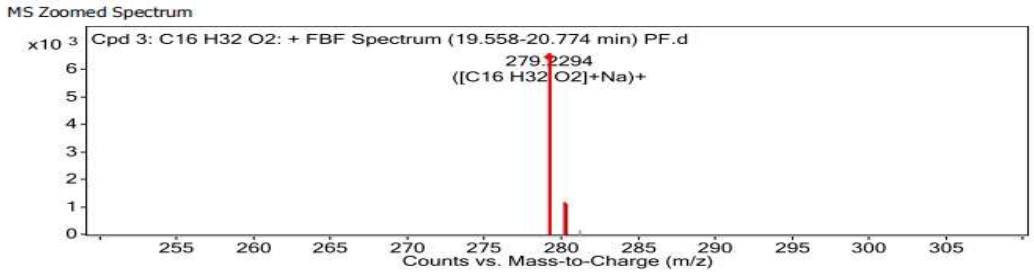

Fig. 4.37: Palmitic acid

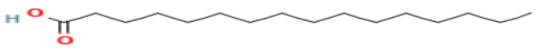

Fig. 4.37a: Structure of Palmitic acid

Anti-phytopathogenic compounds by LC MS TOF with Chemical Structure - Positive Mode

Sl.No.	Compounds	Molecular Formula	Molecular Mass	m/z	RT (min.)
1	2',3'-Dihydroxyacetophenone	$C_8 H_8 O_3$	152.0429	175.0358	1.122
2	Metsulfovax	$C_{12} H_{12} N_2 O S$	232.0684	233.0769	1.141
3	Hypoglycin	$C_7 H_{11} N O_2$	141.0779	142.0853	1.407
4	Carisoprodol	$C_{12} H_{24} N_2 O_4$	260.171	261.1788	1.446
5	3-Beta,6-beta,Dihydroxynortropane	$C_7 H_{13} N O_2$	143.0941	144.1012	1.477
6	L-isoleucyl-L-proline	$C_{11} H_{20} N_2 O_3$	228.1455	229.1529	1.781
7	Pirbuterol	$C_{12} H_{20} N_2 O_3$	240.1458	241.1531	1.863
8	Procyanidin B7	$C_{30}H_{26}O_{12}$	578.1388	579.1461	4.975
9	Octylamine	$C_8 H_{19} N$	129.151	130.1582	5.227
10	Orotidine	$C_{10} H_{12} N_2 O_8$	288.0612	289.0684	5.553
11	Minoxidil	$C_9 H_{15} N_5 O$	209.1262	210.1334	6.117
12	Furanojaponin	$C_{20} H_{28} O_3$	316.2035	339.1927	6.44
13	Erinapyrone C	$C_8 H_{10} O_5$	186.0536	209.0427	6.656
14	(Z)-3-(1-Formyl-1-propenyl)pentanedioic acid	$C_9 H_{12} O_5$	200.0694	223.0586	7.888
15	11 Beta,17beta-Dihydroxy-9alpha-fluoro-17alpha-methyl-5alpha-androstan-3-one	$C_{20} H_{31} F O_3$	338.2294	339.2367	7.951
16	Talampanel	$C_{19} H_{19} N_3 O_3$	337.1413	338.1485	8.436
17	6-Sulfatoxymelatonin	$C_{13} H_{16} N_2 O_6 S$	328.0691	351.0586	9.31
18	Coriandrone E	$C_{13} H_{12} O_5$	248.0689	271.058	11.307
19	Sphinganine	$C_{16} H_{35} N O_2$	273.265	274.2723	12.76
20	Azafenidin	$C_{15} H_{13} Cl_2 N_3 O_2$	337.0403	338.0471	14.499
21	6-Hydroxy penta 7-decane7-dioic acid	$C_{15} H_{28} O_5$	288.1939	311.1832	14.797
22	Nigakilactone B	$C_{22} H_{32} O_6$	392.219	415.208	15.715
23	Tropacocaine	$C_{15} H_{19} N O_2$	245.1409	246.1468	17.321
24	Brassicanal B	$C_{12} H_{11} N O_2 S$	233.0529	256.0421	19.496
25	Carylophyllene oxide	$C_{15} H_{24} O$	220.1833	243.1723	19.762
26	Monomenthyl succinate	$C_{14} H_{24} O_4$	256.168	279.1572	19.842

27	2-Methyl-1-phenyl-2-propanyl butyrate	$C_{14}H_{20}O_2$	220.1446	243.1339	19.856
28	Eugenol	$C_{10}H_{12}O_2$	164.0833	165.0898	19.859
29	(E,E)-2,4-Decadienoiciso butylamide	$C_{14}H_{25}NO$	223.1945	246.1835	20.099
30	2-Amino-1,2-bis-3-(p-chlorophenyl) ethanol	$C_{14}H_{13}Cl_2NO$	281.0392	304.0282	20.07
31	2,6-Di-tert-butyl-4-ethyl phenol	$C_{16}H_{26}O$	234.1988	257.188	20.815
32	(2R)-3(2-Aminoethoxy)(hydroxy) phosphoryloxy-2 (pentadecanoyloxy) propyl (13Z)-13-docosenoate	$C_{42}H_{82}NO_8P$	759.5732	760.5805	21.708
33	9,10-Dihydroxy-12,13-epoxyoctadecanoate	$C_{18}H_{34}O_5$	330.2388	353.228	13.347
34	Octa decanedioic acid	$C_{18}H_{34}O_4$	314.2432	337.2325	15.935
35	(Z)-13-Oxo-9-octadecenoic acid	$C_{18}H_{32}O_3$	296.2328	297.2402	20.136
36	Vanilpyruvic acid	$C_{10}H_{10}O_5$	210.052	211.0595	5.954
37	Palmitic acid	$C_{16}H_{32}O_2$	256.2402	279.2294	20.136

Table 4: Qualitative Compounds in Positive Mode

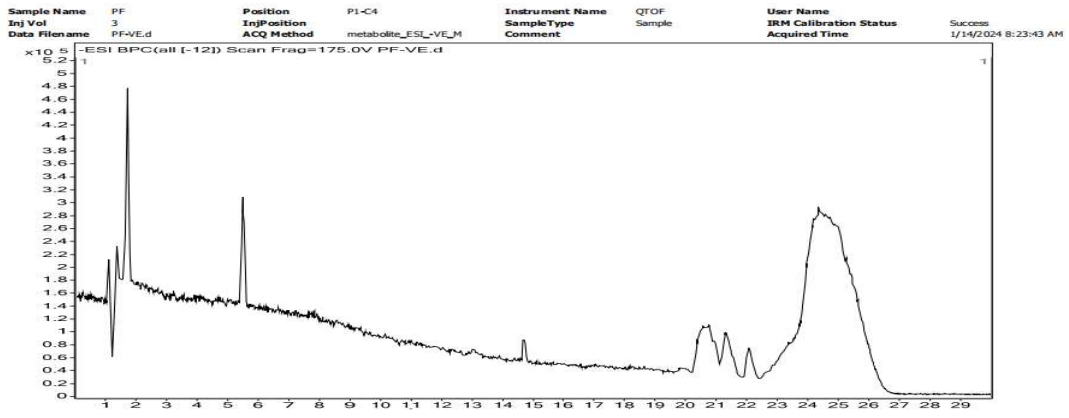

Count vs. Acquisition Time (min.)

Fig. 5: Anti-phytopathogenic compounds with Chemical Structure - Negative Mode

1. Phenyl vinyl sulfide

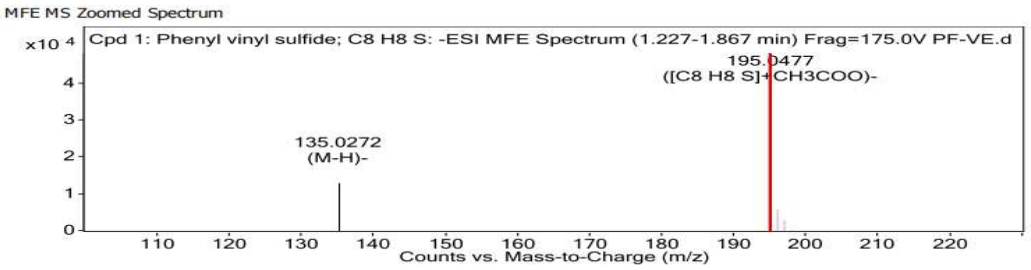

Fig. 5.1: LCMS-QTOF MS: Phenyl vinyl sulfide

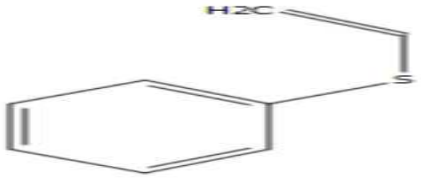

Fig. 5.1a: Structure of Phenyl vinyl sulfide

2. 2-(2-Thienyl) furan

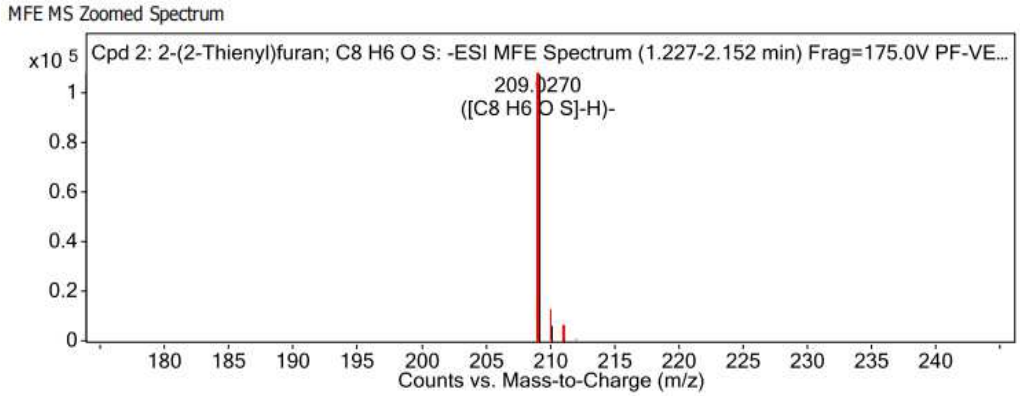

Fig. 5.2: 2-(2-Thienyl) furan

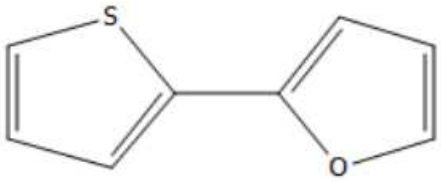

Fig. 5.2a: Structure of 2-(2-Thienyl) furan

3. 2-(Methylthiomethyl)-3-phenyl- 2-propenal

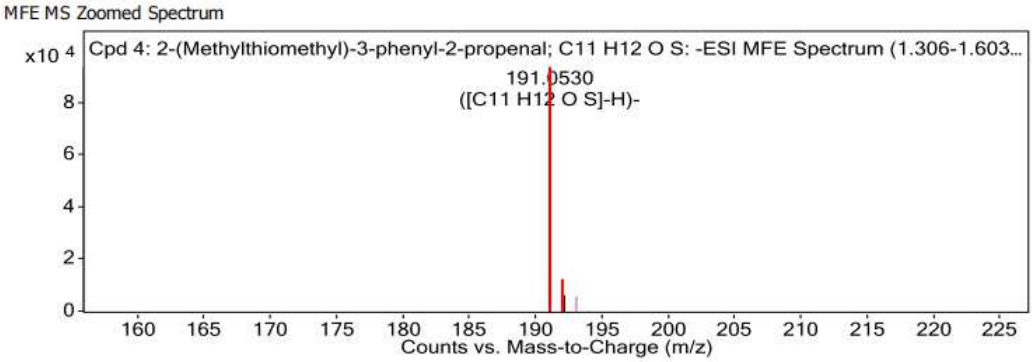

Fig. 5.3: 2-(Methylthiomethyl)-3-phenyl- 2-propenal

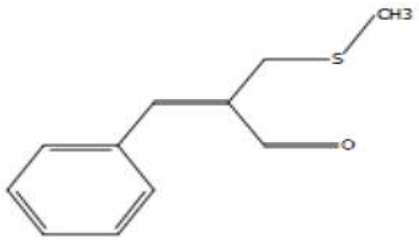

Fig. 5.3a: Structure of 2-(Methylthiomethyl)-3-phenyl- 2-propenal

4. Zapotin

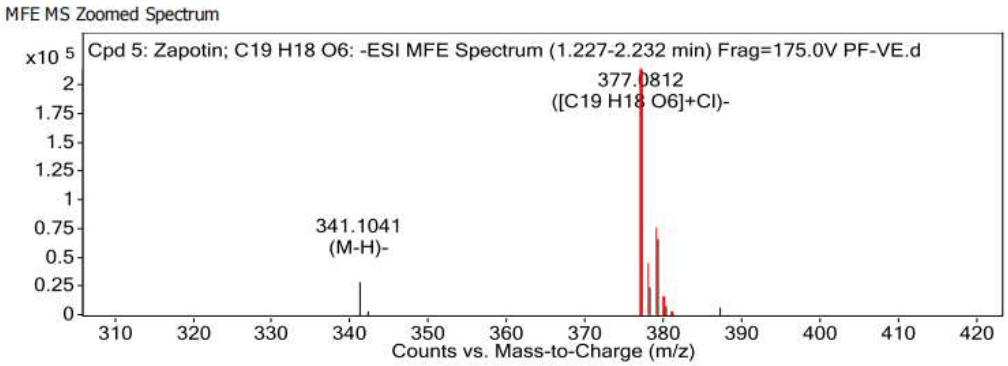

Fig. 5.4: Zapotin

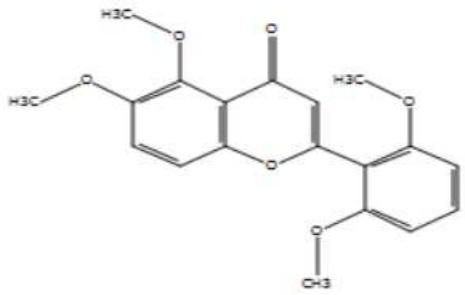

Fig. 5.4a: Structure of Zapotin

5. (Z)-5- [(5-Methyl-2- thienyl) methylene]-2(5H)- furanone

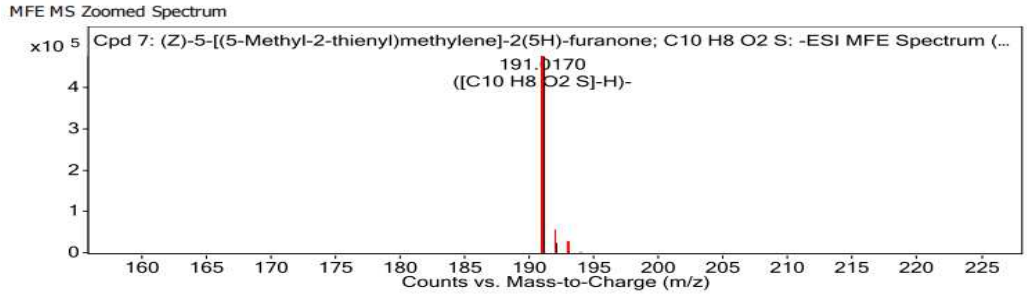

Fig. 5.5: (Z)-5- [(5-Methyl-2- thienyl) methylene]-2(5H) furanone

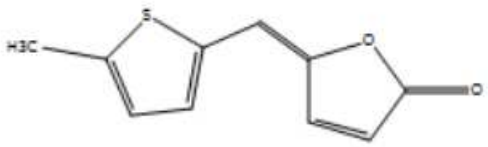

Fig. 5.5a: Structure of (Z)-5- [(5-Methyl-2- thienyl) methylene]-2(5H)- furanone

6. Procyanidin B7

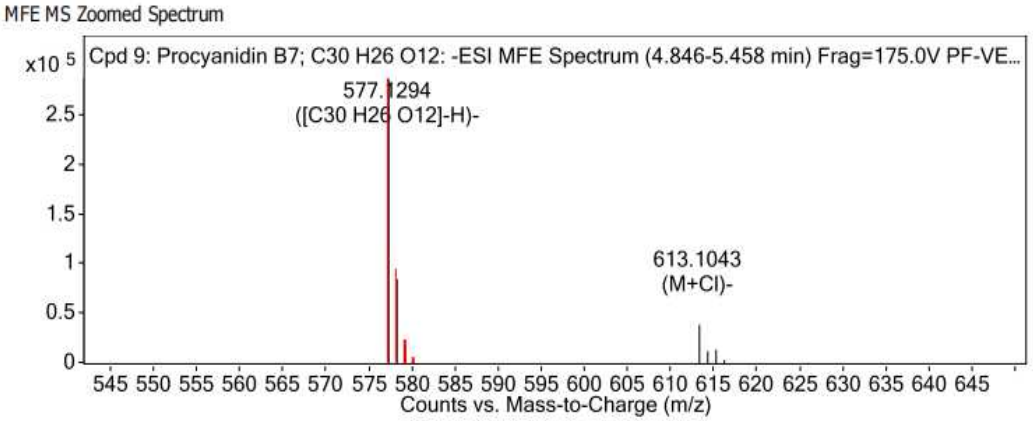

Fig. 5.6: Procyanidin B7

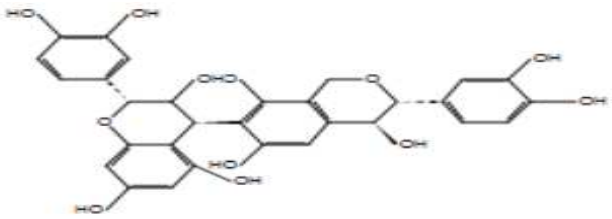

Fig. 5.6a: Structure of Procyanidin B7

7. cis-3,4-Leucopelargonidin

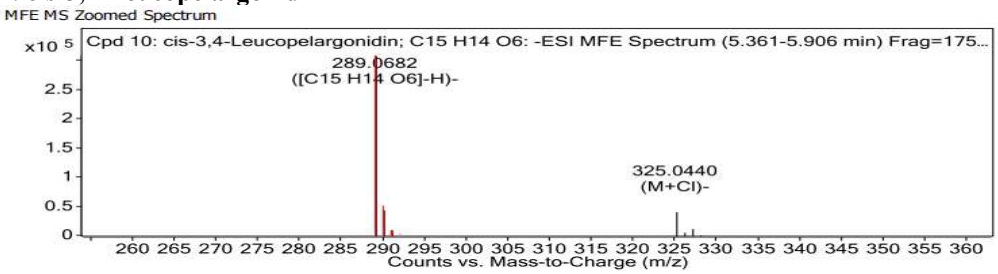

Fig. 5.7: cis-3,4-Leucopelargonidin

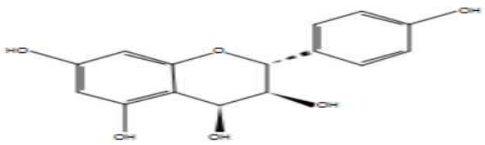

Fig. 5.7a: Structure of cis-3,4-Leucopelargonidin

8. 9S,12S,13S-trihydroxy-10E-octadecenoic acid

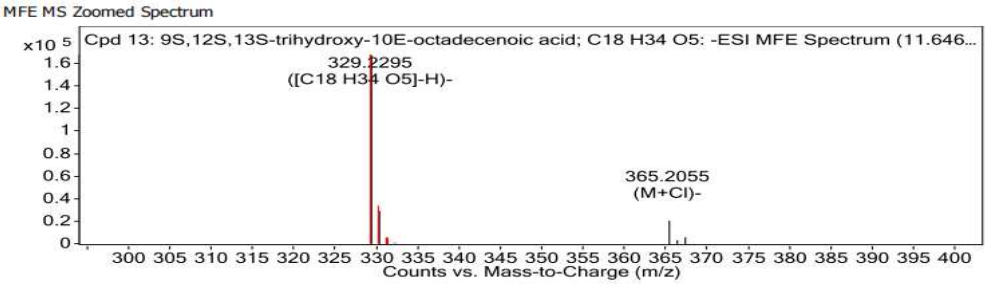

Fig. 5.8: 9S,12S,13S-trihydroxy-10E-octadecenoic acid

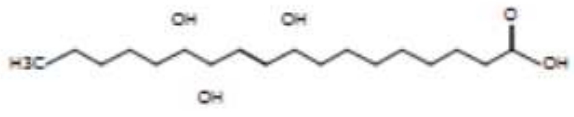

Fig. 5.8a: Structure of 9S,12S,13S-trihydroxy-10E - octadecenoic acid

9. Momordicin II

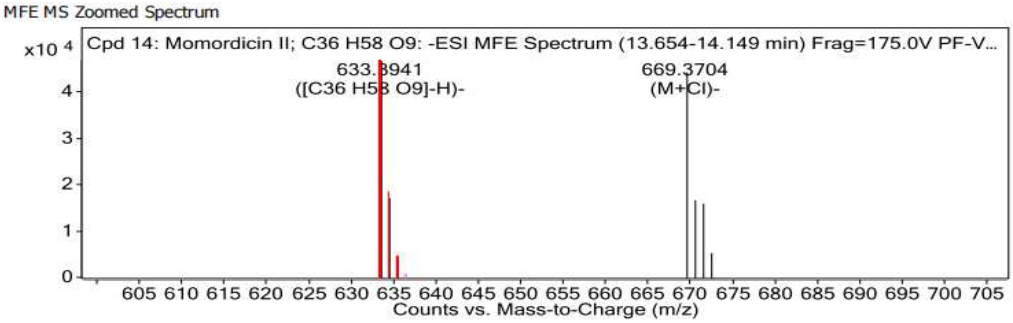

Fig. 5.9: Momordicin II

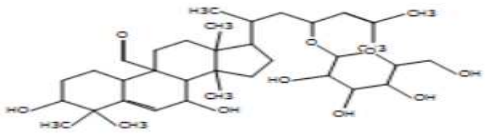

Fig. 5.9a: Structure of Momordicin II

10. Capreomycin

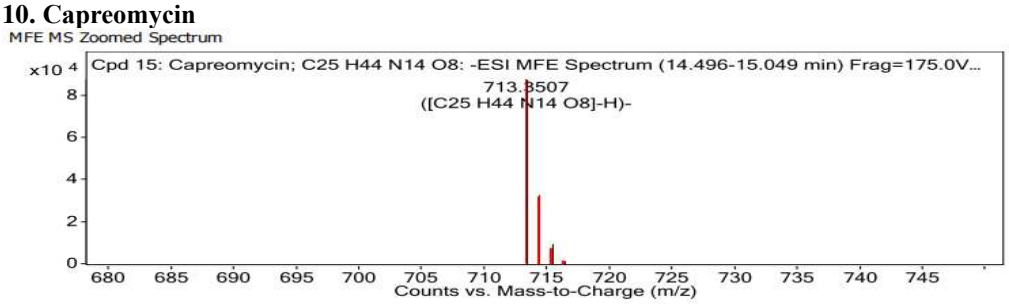

Fig. 5.10: Capreomycin

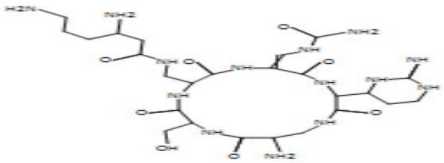

Fig. 5.10a: Structure of Capreomycin

11.4,4-Difluoro-17beta-hydroxy- 17alpha-methyl-androst-5-en-3-one

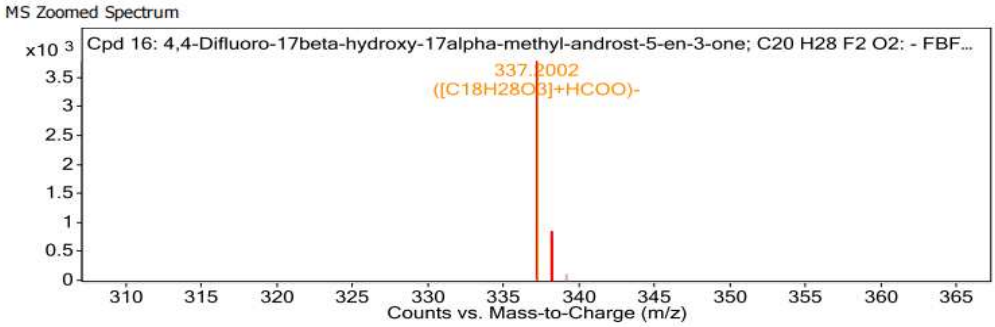

Fig. 5.11: 4,4-Difluoro-17beta-hydroxy- 17alpha-methyl-androst-5-en-3-one

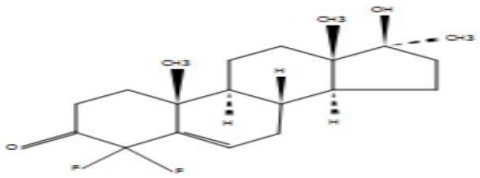

Fig. 5.11a: Structure of 4,4-Difluoro-17beta-hydroxy- 17alpha-methyl-androst-5-en-3-one

3.3.2. Anti-phytopathogenic Qualitative Compounds by LC MS TOF in Negative Mode

Sl. No.	Compounds	Molecular Formula	Molecular Mass	m/z	RT (min)
1	Phenyl vinyl sulfide **T**	C_8H_8S	136.0339	195.0477	1.379
2	2-(2-Thienyl) furan	C_8H_6OS	150.01033	209.027	1.392
3	2-(Methylthiomethyl)-3-phenyl- 2-propenal	$C_{11}H_{12}OS$	192.0603	191.053	1.414
4	Zapotin	$C_{19}H_{18}O_6$	342.1117	377.0812	1.417
5	(Z)-5- [(5-Methyl-2- thienyl) methylene]-2(5H)- furanone	$C_{10}H_8O_2S$	192.0243	191.017	1.742
6	Procyanidin B7	$C_{30}H_{26}O_{12}$	578.1365	577.1294	4.993
7	Cis-3,4-Leucopelargonidin	$C_{15}H_{14}O_6$	290.0754	289.0682	5.522
8	9S,12S,13S-Trihydroxy-10E - octadecenoic acid	$C_{18}H_{34}O_5$	330.2367	329.2295	11.87
9	Momordicin II	$C_{36}H_{58}O_9$	634.4012	633.3941	13.783
10	Capreomycin	$C_{25}H_{44}N_{14}O_8$	668.3524	713.3507	14.715
11	4,4-Difluoro-17beta-hydroxy- 17alpha-methyl-androst-5-en- 3-one	$C_{20}H_{28}F_2O_2$	338.2074	337.2002	24.973

Table 5: Compounds in Negative Mode

4. Discussion

This study focused on isolating and characterizing plant growth-promoting rhizobacteria (PGPR) from Kerala's rhizospheric soils. Ten of the 90 bacterial strains were selected for their plant growth-promoting (PGP) traits. These results are consistent with research showing that PGPR promotes plant development via various methods, which is important for sustainable agriculture[18,49,50,53]. IAA, a crucial phytohormone that encourages root growth and elongation, was produced by two isolates. The reaction with the Salkowski reagent confirmed their ability to synthesize IAA in the presence of L-Tryptophan. Reported[48] similar results with PGPR isolated from the *Pterocarpus marsupium* rhizosphere, which enhanced wheat seedling growth. Phosphorus is critical for plant growth and the Fa strains in this study exhibited phosphate solubilization activity. *Pseudomonas fluorescens* (P80) showed the highest solubilization (308 mg/L) and a pH reduction to 3.0. These results align with[7,55], who reported significant phosphate solubilization by fluorescent *Pseudomonads*. ACC deaminase-producing PGPR mitigates stress-induced growth inhibition by reducing plant ethylene levels. *Pseudomonas fluorescens* (P80) and *Bacillus subtilis* exhibited ACC deaminase activity. Reported[33,8]

similar results, demonstrating improved root development and reduced downy mildew severity in plants treated with PGPR. Siderophore production enhances plant iron uptake. *Pseudomonas fluorescens* (P80) exhibited this trait, with P80 showing the highest activity. Reported[55,36] that *Pseudomonas* species are robust siderophore producers, benefiting plant health and competitiveness in the rhizosphere. Among the two isolates, only P80 exhibited nitrogen-fixing ability. Demonstrate[71,19] that PGPR inoculation reduces nitrogen fertilizer dependency while maintaining crop yield, reinforcing the potential of nitrogen-fixing PGPR as biofertilizers. Isolates, including *Pseudomonas fluorescens* and *Bacillus subtilis*, demonstrated ammonia production. Reported[36,1] similar findings, suggesting that ammonia-producing PGPR can contribute to nitrogen enrichment and promote plant growth. HCN production by PGPR suppresses phytopathogens. P80 exhibited HCN production[43,57] highlighted the biocontrol potential of HCN-producing PGPR in pathogen suppression. Potassium solubilization enhances plant resilience against environmental stresses. P80 exhibited this activity, which aligns with[13], who reported similar findings in *Actinobacteria* strains. P80 was Gram-negative and P75 Ca was Gram-positive. Most exhibited catalase and citrate utilization activity, while some tested positive for urease, oxidase and nitrate reduction. Reported[70,61] similar biochemical characteristics in PGPR isolates, highlighting their diverse metabolic capabilities. 16S rDNA sequencing, confirmed the two isolates, including P80 and P75; similar molecular characterization studies by[22,17] validated the genetic diversity of PGPR strains, confirming their potential as biofertilizers. *Pseudomonas fluorescens* and its crude extracts exhibited antiphytopathogenic activity against *Sclerotium rolfsii, Phytophthora infestans, Fusarium oxysporum* and *Fusarium solani*. Reported[45,38] similar antifungal activity from *P. fluorescens* isolates. Thin-layer chromatography (TLC) identified antifungal compounds at Rf 0.28, inhibiting several plant pathogens. Demonstrated[50], that *P. fluorescens* isolates from rice rhizosphere re-suppressed *Magnaporthe grisea* and *Rhizoctonia solani*. Ethyl acetate extraction and TLC analysis identified antifungal compounds at Rf 0.22, 0.35, 0.42 and 0.51, with a specific compound at Rf 0.35 completely inhibiting fungal growth. Confirmed[45] that *P. fluorescens* crude extracts exhibited broad-spectrum inhibition against multiple plant pathogens. LC-MS/MS analysis identified five phenazine derivatives in *Pseudomonas* strains, including phenazine-1-carboxylic acid (PCA) and 2-hydroxyphenazine[56]. Tested[51] *P. fluorescens* against ten fungal pathogens and identified phenol 2,4-bis (1,1-dimethylethyl) as the active antifungal component. In the present study, LC-QTOF-MS of column chromatography fractions identified 37 compounds in positive mode and 11 in negative mode. The study confirmed that the isolated PGPR exhibits multiple plant growth-promoting traits, including IAA production, phosphate solubilization, ACC deaminase activity, siderophore production, nitrogen fixation, ammonia production, HCN production and potassium solubilization. These findings suggest that the identified PGPR isolates have significant potential for agricultural applications. Further field trials and bioformulation development will be necessary to evaluate their efficacy under different environmental conditions.

5. Conclusions and Future Perspectives

PGPRs offer a safe and effective approach to enhancing agricultural productivity while reducing reliance on synthetic inputs; as key components of rhizosphere engineering, PGPRs improve plant growth, mitigate stress and regulate plant diseases. Over the past few decades, extensive research has identified and optimized PGPR strains for diverse crops and environmental conditions. PGPRs enhance nutrient availability and phytohormone production and support plant resilience against abiotic stress. Their potential to replace chemical fertilizers and pesticides makes them crucial for sustainable agriculture. However, further research is needed to develop optimized strains adaptable to agroecological settings. Harnessing microbial potential can lead to innovative biotechnological applications, such as biofertilizers and biopesticides, which promote plant growth and phytoremediation. Advancements in soil fertility, plant tolerance and nutrient cycling demonstrate PGPRs' role in sustainable farming. Integrating modern technologies with PGPR research will improve their effectiveness, ensuring long-term agricultural sustainability.

Ethics approval and consent to participate
Not applicable.
Consent for publication
Not applicable.

Authors' Contributions
ST and LM designed the study and provided all the data. LM supervised the project development. ST

conducted the data analysis, wrote the draft manuscript and edited the final version. All authors read and approved the final manuscript.

Acknowledgment:
I sincerely thank Prof. Dr. Lizzy Mathew, Department of Botany and Centre for Research, St. Teresa's College, Ernakulam and Prof. Dr. K. Surendra Gopal, Head, Department of Agricultural Microbiology, College of Agriculture, Vellanikkara, Thrissur, Kerala for their invaluable guidance and support.

Funding:
This research was financially supported by the Directorate of Collegiate Education, Government of Kerala, under the DCE Aspire Award (2022–23).

Conflict of Interest:
The authors declare no competing interests.

CRediT authorship contribution statement

Smitha Thomas: Conceptualization, Methodology, Software **Smitha Thomas**: Data curation, Writing- Original draft preparation. **Smitha Thomas**: Visualization, Investigation. **Lizzy Mathew***:* Supervision.**: Smitha Thomas**: Software, Validation.: **Lizzy Mathew:** Writing-Reviewing and Editing,

References:

1. Agbodjato, N.A., Noumavo, P.A., Baba-Moussa, F., Salami, H.A., Sina, H., Sèzan, A., Bankolé, H., Adjanohoun, A. and Baba-Moussa, L., 2015. Characterization of potential plant growth promoting rhizobacteria isolated from Maize (Zea mays L.) in central and Northern Benin (West Africa). *Applied and Environmental Soil Science*, *2015*(1), p.901656.
2. Aluko, O.O., Kant, S., Adedire, O.M., Li, C., Yuan, G., Liu, H., Wang, Q., 2023. Unlocking the potentials of nitrate transporters at improving plant nitrogen use efficiency. *Front. Plant Sci*. 14, 107–4839.
3. Angulo, V., Beriot, N., Garcia-Hernandez, E., Li, E., Masteling, R., Lau, J.A., 2022. Plant–microbe eco-evolutionary dynamics in a changing world. *New Phytologist* 234, 1919–1928.
4. Astapati, A.D., Nath, S., 2023. The complex interplay between plant-microbe and virus interactions in sustainable agriculture: harnessing phytomicrobiomes for enhanced soil health, designer plants, resource use efficiencyand food security. *Crop Des.* 2, 100028.
5. Backer, R., Rokem, J.S., Ilangumaran, G., Lamont, J., Praslickova, D., Ricci, E., Subramanian, S., Smith, D.L., 2018. Plant growth-promoting rhizobacteria: context, mechanisms of actionand roadmap to commercialization of biostimulants for sustainable agriculture. *Front. Plant Sci.* 9, 1473.
6. Bakker, P. A., Doornbos, R. F., Zamioudis, C., Berendsen, R. L.and Pieterse, C. M. (2013). Induced systemic resistance and the rhizosphere microbiome. *The plant pathology journal*, *29*(2), 136.
7. Bakki M, Banane B, Marhane O, Esmaeel Q, Hatimi A, Barka EA, Azim K and Bouizgarne B (2024) Phosphate solubilizing *Pseudomonas* and *Bacillus* combined with rock phosphates promoting tomato growth and reducing bacterial canker disease. *Front. Microbiol.* 15:1289466. doi: 10.3389/fmicb.2024.1289466.
8. Barnawal, D., Singh, R.and Singh, R. P. (2019). Role of plant growth promoting rhizobacteria in drought tolerance: regulating growth hormones and osmolytes. In *PGPR amelioration in sustainable agriculture* (pp. 107-128). Woodhead Publishing.
9. Bastías, D.A., Applegate, E.R., Johnson, L.J., Card, S.D., 2022. Factors controlling the effects of mutualistic bacteria on plants associated with fungi. *Ecol. Lett.* 25, 1879–1888.
10. Bazany, K.E., Wang, J.T., Delgado-Baquerizo, M., Singh, B.K., Trivedi, P., 2022. Water deficit affects inter-kingdom microbial connections in plant rhizosphere. *Environ. Microbiol.* 24, 3722–3734.

11. Bender, S.F., Wagg, C., van der Heijden, M.G., 2016. An underground revolution: biodiversity and soil ecological engineering for agricultural sustainability. Trends Ecol. Evol. (Amst.) 31, 440–452.
12. Bhat, B.A., Tariq, L., Nissar, S., Islam, S.T., Islam, S.U., Mangral, Z., Ilyas, N., Sayyed, R. Z., Muthusamy, G., Kim, W., 2022. The role of plant-associated rhizobacteria in plant growth, biocontrol and abiotic stress management. *J. Appl. Microbiol.* 133, 2717–2741.
13. Boubekri, K., Soumare, A., Mardad, I., Lyamlouli, K., Hafidi, M., Ouhdouch, Y. and Kouisni, L., 2021. The screening of potassium-and phosphate-solubilizing actinobacteria and the assessment of their ability to promote wheat growth parameters. *Microorganisms*, *9*(3), p.470.
14. Calvo, P., Zebelo, S., McNear, D., Kloepper, J., Fadamiro, H., 2019. Plant growth promoting rhizobacteria induce changes in Arabidopsis thaliana gene expression of nitrate and ammonium uptake genes. *J. Plant Interact.* 14, 224-231.
15. Carreiras, J., Cruz-Silva, A., Fonseca, B., Carvalho, R.C., Cunha, J.P., Proença Pereira, J., Paiva-Silva, C., A. Santos, S., Janeiro Sequeira, R., Mateos-Naranjo, E., 2023. Improving grapevine heat stress resilience with marine plant growth-promoting rhizobacteria consortia. Microorganisms 11, 856.
16. Castro, D., 2022. Who comes first? Implications of the plant-microbiome-soil continuum feedback on plant performance. *Acta Uni Agri Sueciae.* 27.
17. Chamkhi, I., Sbabou, L.and Aurag, J. (2023). Improved growth and quality of saffron (*Crocus sativus* L.) in the field conditions through inoculation with selected native plant growth-promoting rhizobacteria (PGPR). *Industrial Crops and Products*, *197*, 116606.
18. Chanway, C. P., Hynes, R. K.and Nelson, L. M. (1989). Plant growth-promoting rhizobacteria: effects on growth and nitrogen fixation of lentil (Lens esculenta Moench) and pea (*Pisum sativum* L.). *Soil Biology and Biochemistry*, *21*(4), 511-517.
19. Chebotar, V. K., Chizhevskaya, E. P., Vorobyov, N. I., Bobkova, V. V., Pomyaksheva, L. V., Khomyakov, Y. V.and Konovalov, S. N. (2022). The quality and productivity of strawberry (Fragaria× ananassa Duch.) improved by the inoculation of PGPR *Bacillus velezensis* BS89 in field experiments. *Agronomy*, *12*(11), 2600.
20. Cordero, A.P., Vergara, D.E.M., Mendoza, Y.A., 2023. Production of 1-aminocyclopropane-1-carboxylic acid deaminase (ACC) by *Burkholderia cepacia* as an indicator of cadmium contamination. *J. Posit. Sch. Psychol.* 1008–1016.
21. Costantini, E.A., Mocali, S., 2022. Soil health, soil genetic horizons and biodiversity#. Plant Nutr. Soil Sci. 185, 24–34.
22. Das, S., Vaishnavee, V. H. S., Dedha, A., Yadav, P., Singh, R. P.and Kumar, A. (2024). PGPRs: Toward a Better Greener Future in Sustainable Agriculture. *Microbes Based Approaches for the Management of Hazardous Contaminants*, 397-410.
23. Dhole, A.M., Shelat, H.N., Patel, H.K., Jhala, Y.K., 2023. Evaluation of the Co-inoculation Effect of Rhizobium and Plant Growth Promoting Non-rhizobial Endophytes on *Vigna radiata.* Curr. *Microbiol.* 80, 167.
24. Dhungana, I., Kantar, M.B., Nguyen, N.H., 2023. Root exudate composition from different plant species influences the growth of rhizosphere bacteria. *Rhizosphere* 25, 100645.
25. Díaz, M., Bach, T., Anta, G.G., Agaras, B., Wibberg, D., Noguera, F., Canciani, W., Valverde, C., 2022. Agronomic efficiency and genome mining analysis of the wheat biostimulant rhizospheric bacterium *Pseudomonas pergaminensis* sp. nov. strain 1008T. *Front. Plant Sci.* 13.
26. Etesami, H., Adl, S.M., 2020. Plant growth-promoting rhizobacteria (PGPR) and their action mechanisms in availability of nutrients to plants. In: Phyto-Microbiome in Stress Regulation, pp. 147–203.
27. Farhat, F., Tariq, A., Waseem, M., Masood, A., Raja, S., Ajmal, W., Iftikhar, I., Zulfiqar, U., Maqsood, M.F., 2023. Plant Growth Promoting Rhizobacteria (PGPR) Induced Improvements in the Growth, Photosynthesis, Antioxidants, and Nutrient Uptake of Rapeseed (*Brassica napus* L.). *Gesunde Pflanzen* 1–14.
28. Fazeli-Nasab, B., Sayyed, R. Z., Piri, R.and Rahmani, A. F. (2021). Biopriming and nanopriming: green revolution wings to increase plant yield, growthand development under stress condition and forward dimensions. *Antioxidants in plant-microbe interaction*, 623-655.
29. Goswami, D., Thakker, J. N.and Dhandhukia, P. C. (2016). Portraying mechanics of plant growth promoting rhizobacteria (PGPR): a review. *Cogent Food and Agriculture*, *2*(1), 1127500.
30. Gupta, S., Pandey, S., 2023. Plant growth promoting rhizobacteria to mitigate biotic and abiotic stress in plants. In: *Sustainable Agriculture Reviews* 60: Microbial Processes in Agriculture, pp. 47–68.

31. Hartman, K.and Tringe, S. G. (2019). Interactions between plants and soil shaping the root microbiome under abiotic stress. *Biochemical Journal*, *476*(19), 2705-2724.
32. Hao, C., Dungait, J.A., Wei, X., Ge, T., Kuzyakov, Y., Cui, Z., Tian, J. and Zhang, F., 2022. Maize root exudate composition alters rhizosphere bacterial community to control hotspots of hydrolase activity in response to nitrogen supply. *Soil Biology and Biochemistry*, *170*, p.108717.
33. Hassen, W., Neifar, M., Cherif, H., Najjari, A., Chouchane, H., Driouich, R.C., Salah, A., Naili, F., Mosbah, A., Souissi, Y. and Raddadi, N., 2018. *Pseudomonas rhizophila* S211, a new plant growth-promoting rhizobacterium with potential in pesticide-bioremediation. *Frontiers in Microbiology*, *9*, p.34.
34. Jafari, M., Tahmoures, M., Ehteram, M., Ghorbani, M., Panahi, F., 2022. The role of vegetation in confronting erosion and degradation of soil and land. Soil Erosion Control in Drylands. *Springer*, pp. 33–141.
35. Jalal, A., da Silva Oliveira, C.E., Galindo, F.S., Rosa, P.A.L., Gato, I.M.B., de Lima, B.H., Teixeira Filho, M.C.M., 2023. Regulatory mechanisms of plant growth-promoting rhizobacteria and plant nutrition against abiotic stresses in Brassicaceae family. Life 13, 211.
36. Joseph, B., Patra, R. R.and Lawrence, R. (2007). Characterization of plant growth promoting rhizobacteria associated with chickpea (*Cicer arietinum* L.). *International Journal of Plant Production*, *1*(2), 141-152.
37. Kechid, M., Desbrosses, G., Gamet, L., Castaings, L., Varoquaux, F., Djekoun, A., Touraine, B., 2022. Arabidopsis growth-promotion and root architecture responses to the beneficial rhizobacterium *Phyllobacterium brassicacearum* Strain STM196 are independent of the nitrate assimilatory pathway. *Plants* 11, 128.
38. Koche, M. D., Gade, R. M.and Deshmukh, A. G. (2012). Antifungal activity of secondary metabolites produced by *Pseudomonas fluorescens*. *Pesticide Research Journal*, *24*(1), 21-24.
39. Kour, D., Kaur, T., Devi, R., Chaubey, K.K., Yadav, A.N., 2023. Co-inoculation of nitrogen fixing and potassium solubilizing Acinetobacter sp. for growth promotion of onion (*Allium cepa*). Biologia 1–7.
40. Kumar, D., Saraf, M., Joshi, C.G., Joshi, M., 2022a. Host plant rhizo-microbiome interactions: seasonal variation and microbial community structure analysis associated with *Barleria prionitis*. *Ecol. Genet. Genomics* 22, 100109.
41. Kumar, S., Sindhu, S.S., Kumar, R., 2022b. Biofertilizers: an ecofriendly technology for nutrient recycling and environmental sustainability. *Curr. Res. Microb. Sci.* 3, 100094.
42. Liu, Q., Wu, K., Song, W., Zhong, N., Wu, Y., Fu, X., 2022. Improving crop nitrogen use efficiency toward sustainable green revolution. Annu. Rev. *Plant Biol.* 73, 523–551.
43. Maral-Gül, D.and Eltem, R. (2024). Evaluation of Bacillus isolates as a biological control agents against soilborne phytopathogenic fungi. *International Microbiology*, 1-15.
44. Mashabela, M.D., Piater, L.A., Dubery, I.A., Tugizimana, F., Mhlongo, M.I., 2022. Rhizosphere tripartite interactions and PGPR-mediated metabolic reprogramming towards ISR and plant priming: a metabolomics review. *Biology* (Basel) 11, 346.
45. Mohamed, H., El-Shanawany, A.R., Shah, A.M., Nazir, Y., Naz, T., Ullah, S., Mustafa, K. and Song, Y., 2020. Comparative analysis of different isolated oleaginous Mucoromycota fungi for their γ-Linolenic acid and carotenoid production. *BioMed Research International*, *2020*(1), p.3621543.
46. Nagrale, D., Chaurasia, A., Kumar, S., Gawande, S., Hiremani, N., Shankar, R., GokteNarkhedkar, N., Prasad, Y., 2023. PGPR: the treasure of multifarious beneficial microorganisms for nutrient mobilization, pest biocontrol and plant growth promotion in field crops. *World J. Microbiol. Biotechnol.* 39, 1–18.
47. Office, M.E., 2019. Erratum: Mpanga, IK; et al. The Form of N Supply Determines Plant Growth Promotion by P-Solubilizing Microorganisms in Maize. *Microorganisms* 2019, 7, 38. Microorganisms 7, 111.
48. Randive, V. S., Agnihotri, S. N.and Bhagat, R. B. (2024). Screening and Optimization of IAA Production by PGPR Isolated from Rhizosphere of a *Pterocarpus marsupium* Roxb. and their Effect on Plant Growth. *Current Agriculture Research Journal*, *12*(1).
49. Reddy, P. P.and Reddy, P. P. (2013). Plant growth-promoting rhizobacteria (PGPR). *Recent advances in crop protection*, 131-158.
50. Reddy, K., Choudary, A. K.and Reddy, M. S. (2007). Antifungal metabolites of *Pseudomonas fluorescens* isolated from rhisosphere of rice crop. *J. Mycol Pl Pathol*, *37*(2), 5.
51. Ren, J., Wang, J., Karthikeyan, S., Liu, H.and Cai, J. (2019). Natural anti-phytopathogenic fungi compound phenol, 2, 4-bis (1, 1-dimethylethyl) from *Pseudomonas fluorescens* TL-1.

52. Saghafi, D., Ghorbanpour, M., Shirafkan Ajirloo, H., Asgari Lajayer, B., 2019. Enhancement of growth and salt tolerance in *Brassica napus* L. seedlings by halotolerant Rhizobium strains containing ACC-deaminase activity. *Plant Physiol.* Rep. 24, 225–235.
53. Saini, P.and Khanna, V. (2012). Evaluation of native rhizobacteria as promoters of plant growth for increased yield in lentil (Lens culinaris). *Recent Res. Sci. Technol*, *4*(4), 05-09.
54. Salwan, A. M. Effect of interaction between two types of mycorrhizae and vermicompost on soil biological traits and growth of corn plant.
55. Sayyed, R. Z., Chincholkar, S. B., Reddy, M. S., Gangurde, N. S.and Patel, P. R. (2012). Siderophore producing PGPR for crop nutrition and phytopathogen suppression. In *Bacteria in agrobiology: disease management* (pp. 449-471). *Berlin, Heidelberg: Springer Berlin Heidelberg*.
56. Shahid, I., Han, J., Hardie, D., Baig, D. N., Malik, K. A., Borchers, C. H.and Mehnaz, S. (2021). Profiling of antimicrobial metabolites of plant growth promoting *Pseudomonas* sp. isolated from different plant hosts. *3 Biotech*, *11*, 1-14.
57. Shaikh, S. S., Sayyed, R. Z.and Reddy, M. S. (2016). Plant growth-promoting rhizobacteria: an eco-friendly approach for sustainable agroecosystem. *Plant, soil and microbes: volume 1: implications in crop science*, 181-201.
58. Sharp, C., Foster, K.R., 2022. Host control and the evolution of cooperation in host microbiomes. Nat. Commun. 13, 3567.
59. Sharma, I., Sharma, S., Sharma, V., Singh, A.K., Sharma, A., Kumar, A., Singh, J. and Sharma, A., 2024. PGPR-Enabled bioremediation of pesticide and heavy metal-contaminated soil: A review of recent advances and emerging challenges. *Chemosphere*, p.142678.
60. Sharma, M., Bhardwaj, R., Saran, M., Prajapat, R.K., Sharma, D., Mathur, M., 2023. Secondary metabolites and bioprospecting. In: Plant Growth Promoting Microorganisms of Arid Region. *Springer*, pp. 229–255.
61. Shobha, G.and Kumudini, B. S. (2012). Antagonistic effect of the newly isolated PGPR *Bacillus* sp. on Fusarium oxysporum. *Int J Appl Sci Eng Res*, *1*(3), 463-474.
62. Sulieman, S., 2019. Complex dynamics and synchronization of N-feedback and C alteration in the nodules of Medicago truncatula under abundant N or sub-optimal P supply. In: The Model Legume Medicago truncatula, pp. 674–680.
63. Sun, W.and Shahrajabian, M. H. (2025). Biostimulant and beyond: Bacillus spp., the important plant growth-promoting rhizobacteria (PGPR)-based biostimulant for sustainable agriculture. *Earth Systems and Environment*, 1-34.
64. Turan, M., Arjumend, T., Argın, S., Yıldırım, E., Katırcıoglu, ˘ H., Gürkan, B., Ekinci, M., Günes, A., Kocaman, A., Bolouri, P., 2021. Plant root enhancement by plant growth promoting rhizobacteria. *Plant Roots* 2021.
65. Upadhyay, S.K., Rajput, V.D., Kumari, A., Espinosa-Saiz, D., Menendez, E., Minkina, T., Dwivedi, P., Mandzhieva, S., 2022. Plant growth-promoting rhizobacteria: a potential bio-asset for restoration of degraded soil and crop productivity with sustainable emerging techniques. *Environ. Geochem*. Health 1–24.
66. Uzma, M., Iqbal, A., Hasnain, S., 2022. Drought tolerance induction and growth promotion by indole acetic acid producing *Pseudomonas aeruginosa* in Vigna radiata. PLoS ONE 17, e0262932.
67. Vocciante, M., Grifoni, M., Fusini, D., Petruzzelli, G., Franchi, E., 2022. The role of plant growth-promoting rhizobacteria (PGPR) in mitigating plant's environmental stresses. *Appl. Sci*. 12, 1231.
68. Wang, X., Memon, S.P., Panhwar, Q.A., Qasim, M., Younas, M.U., Naher, U.A., 2023b. Biomolecular characterization of salt tolerant plant growth promoting Rhizobacteria isolated from Spinach (*Spinacia oleracea* L.) grown in saline soil.
69. Weemstra, M., Valverde-Barrantes, O.J., McCormack, M.L., Kong, D., 2022. Root Traits and Functioning: From Individual Plants to Ecosystems. *Authorea Preprints*.
70. Yadav, V. K., Gaur, V.and Singh, I. V. (2022). Combined effect of residual and mean stresses on fatigue behavior of welded aluminum 2024 alloy. *International Journal of Fatigue*, *155*, 106565.
71. Zhang, G., Raza, W., Wang, X., Ran, W.and Shen, Q. (2012). Systemic modification of cotton root exudates induced by arbuscular mycorrhizal fungi and *Bacillus vallismortis* HJ-5 and their effects on Verticillium wilt disease. *Applied Soil Ecology*, *61*, 85-91.